

H. KOUTS, R. SHER, J. R. BROWN, D. KLEIN, S. STEIN, R. L. HELLENS, H. ARNOLD, R. M. BALL, AND P. W. DAVIDSON, "PHYSICS OF SLIGHTLY ENRICHED, NORMAL WATER LATTICES (THEORY AND EXPERIMENT)," IN PROCEEDINGS OF THE SECOND INTERNATIONAL CONFERENCE ON THE PEACEFUL USES OF ATOMIC ENERGY, GENEVA, 1957 (UNITED NATIONS, NEW YORK, 1958), VOL. 12, PP. 446-482.

**Proceedings of the Second
United Nations International Conference
on the Peaceful Uses of Atomic Energy**

**Held in Geneva
1 September - 13 September 1958**

**Volume 12
Reactor Physics**



UNITED NATIONS

Geneva
1958

A/CONF.15/1 English, Vol. 12

UNITED NATIONS PUBLICATION

Sales No.: 58.IX.2. Vol. 12

**Price: \$U.S.18.50; £6 12s. (stg.); Sw. fr. 80.00
(or equivalent in other currencies)**

PRINTED IN GREAT BRITAIN

Physics of Slightly Enriched, Normal Water Lattices (Theory and Experiment)

By H. Kouts,* R. Sher,* J. R. Brown,† D. Klein,† S. Stein,† R. L. Hellens,‡ H. Arnold,§
R. M. Ball|| and P. W. Davison§

The three years since the last Geneva conference have seen a notable improvement in the knowledge and understanding of the neutron behavior of reactor cores of slightly enriched uranium in light water. During this interval, the measurements of the parameters have been improved and extended, so that the body of data against which methods of analysis can be tried is now quite large. Not all interesting situations and conditions are covered by the range of completed experiments, and so there is likely to be activity in this field for still a few more years.

The methods of calculation used for finding the critical parameters and the relative reaction rates have undergone a great deal of change. It has become apparent that the classical ways by which these quantities were calculated would not suffice, for they do not permit analysis of multi-region systems or of reactor cores in which a substantial amount of burnup has taken place. The theoretical methods have thus been forced to multigroup and related few-group forms, in which the properties of the assemblies are homogenized.

Since both the measurements and the theory are still not completely developed, it would be too much to hope that a progress report of this nature could demonstrate excellent agreement in all respects. Broadly speaking, however, the measured parameters are quite well reproduced by the calculations. It may be expected that this situation will improve even more as methods are made increasingly better.

One definite feature of the incompleteness of this

report is a changing attitude toward neutron leakage and the migration area. This is reflected in a situation where the experiments are still being analyzed by old methods, while at the same time the theory is pointing toward a need for changing to new methods. It is to be expected that the next stage in the improvement of the physical understanding of these systems will be the reconciling of these two points of view.

EXPERIMENTAL SECTION

Definition

It is convenient to define at the beginning a uniform notation for the quantities which have been measured. Furthermore, it is best to choose these quantities to be as nearly as possible those given directly by the experiments. The experimental results expressed this way are readily assimilated into various schemes of calculation being used.

The quantities derived from the experiments are

B^2	The usual material buckling.
λ	The reflector savings when the lattice is immersed in an effectively infinite tank of water. The definition is specified more exactly in the discussion of measurements of B^2 .
f	The thermal utilization (see below).
δ_{28}	The ratio of the fission rate in U^{238} to that in U^{235} .
δ_{25}	The ratio of epi-cadmium to sub-cadmium fission rates in U^{235} .
ρ_{28}	The ratio of epi-cadmium to sub-cadmium capture in U^{238} .
R_{Au}	The cadmium ratio in the fuel of an effectively zero-thickness gold foil.
θ_m	Effective neutron temperature in the moderator.
$d\rho/d\theta$	Temperature coefficient of reactivity.
$d\rho/dB_g^2$	Buckling coefficient of reactivity. B_g^2 is the geometrical buckling, and the coefficient is the change in reactivity per unit change of this size parameter.

The thermal utilization is, as usually defined, the number of thermal neutrons absorbed in the fuel per thermal neutron absorbed in the reactor. Since these

* Brookhaven National Laboratory, hereafter referred to as BNL.

† Westinghouse, Bettis Atomic Power Division, hereafter referred to as Bettis.

‡ Combustion Engineering Corporation.

§ Westinghouse, Atomic Power Division (Yankee Electric Project).

|| Babcock and Wilcox Corporation.

The following additional people contributed materially to the work described in this paper: G. Price,* K. W. Downes,* E. Weinstock,* S. Lukasik,† G. Smith,† J. Volpe,† F. Frantz,† D. Harris,† J. Andrews,† W. Baer,† J. DeJuren,† A. Kranz,† A. I. MacKinnay,† J. H. Mortenson,† D. A. Ross,|| D. V. P. Williams,|| S. S. Berg,§ W. H. Bergmann,§ D. F. Hanlem,§ R. D. Leamer§ and J. E. Howard.¶

¶ Yankee Atomic Electric Company.

lattices consist of fuel, aluminum, and moderator, the expression for the thermal utilization is

$$f = \left(1 + \frac{V_m N_m \bar{\sigma}_m(\theta_m) \phi_m + V_{Al} N_{Al} \bar{\sigma}_{Al}(\theta_{Al}) \phi_{Al}}{V_U [N_{25} \bar{\sigma}_{25}(\theta_U) + N_{28} \bar{\sigma}_{28}(\theta_U)] \phi_U} \right)^{-1}$$

V is the volume of material, N the atomic density, and ϕ_m/ϕ_u the disadvantage factor. The subscripts m, 25, 28, and Al refer to the nuclei which have non-negligible thermal capture cross sections; moderator (hydrogen), U²³⁵, U²³⁸, and aluminum, respectively. Because the thermal flux distributions in the various media are not necessarily maxwellian at room temperature, the parentheses indicate that the cross sections should be averaged over the spectra actually prevailing. ϕ_U is then the effective temperature of the neutron distribution in the rod. The errors in the experimental determinations of f introduced by neglecting the difference in fuel and moderator temperatures have been analyzed both at Bettis and BNL. It has been shown that the techniques used at the two laboratories cause the error from this source to be negligible.^{2,5}

BNL Experiments

Exponential experiments at BNL on light water moderated, slightly enriched uranium rod lattices have been described in detail in Refs. 1 and 2. These earlier measurements have now been extended to smaller rod sizes, and this section will summarize recent results obtained with 0.387 in. diameter rods and, to some extent, 0.250-in. rods.

Except where otherwise noted, the experimental techniques were identical with or similar to those used with larger rod sizes and described in Ref. 1.

The enrichments used were the same as those of the 0.600-in. rods, namely 1.027%, 1.143%, and 1.299% (by weight) of U²³⁵. The rods were clad in 0.028-in. 2S aluminum, with a nominal 0.005-in. air gap between fuel and clad. The water to uranium volume ratios ranged between 1 and 4. The enrichments of the 0.250 in. rods were 1.027% and 1.143% only. Values differ slightly from those in Appendix 1, being the results of different measurements. Hereafter in this report, nominal enrichments only will be used. The water to uranium volume ratio will be denoted by W/U .

The rods used in the course of buckling measurements were 4 ft long, loaded into the exponential experiment facility¹ fed by a thermal column on top of the BNL Research Reactor. Measurements of thermal utilizations, δ_{28} , δ_{25} , R_{Au} , and ρ_{28} were done with "miniature" lattices. These contained relatively small numbers of 18-in.-long rods in a small (12 in. diameter) tank reflected by paraffin. The measurements involved irradiations in a tunnel under the BNL reactor at a thermal neutron flux about 100 times that available in the large facility. Work on the 0.600-in. rods had previously shown that the results obtained using miniature lattices agreed with

those obtained with full-sized assemblies, and were much more conveniently obtained. A critical facility was also used to determine critical masses (for safety purposes) and for certain other critical assembly measurements.

B^2

Material bucklings were obtained in the usual way from axial and radial thermal flux distribution measurements. The axial flux distributions in most of the lattices were measured by activation of indium foils placed either in a sectioned fuel rod or in a plastic rod inserted between fuel rods. The activation took place at or near the center of the lattice. The method, together with its analysis for end effect corrections, is fully described in Ref. 1.

Radial flux distributions in 0.387 in. rod lattices were measured with a small fission chamber inserted in one of the fuel rods. A section of fuel was removed near the center of the rod, and the fission chamber, which was about 2.5 in. long, was inserted at this position. The uranium above the fission chamber was drilled axially to permit the upward passage of cables to the electronic circuitry of the pulse amplification and counting systems. It was hoped that this arrangement would minimize the amount of uranium removed from the lattice. This rod containing the chamber then successively replaced fuel rods along a radius of the lattice. Meanwhile, a second fission chamber in a fixed position in the water reflector monitored the pile power fluctuations. The count rates of the "radial" chamber, normalized to the standard counts of the monitor, were fitted by least squares to the function

$$F(r) = A J_0(\alpha r)$$

for points sufficiently far from the core-reflector boundary for the $I_0(\beta r)$ contribution to be judged negligible. A and α were the constants determined by the fit.

The reflector savings, λ , was calculated by subtracting r_0 , the geometric loaded radius of the core, from the value of r for which the argument of the J_0 function vanished. Since the geometric radius changed with direction (the loading was not perfectly cylindrical), an effective value of r_0 was computed by taking the total area of the core as N times the area of a unit cell (N = number of rods) and equating this area to πr_0^2 .

It eventually proved impractical to build fission counters to fit inside 0.250 in. diameter rods. The radial flux distributions in these lattices are being measured with the aid of small BF₃ counters which displace the uranium from a short length of a fuel element. The wiring for these is ducted in the same way as that for the fission counters. The method of data handling is of course identical with that just described.

Early foil and fission counter measurements of the buckling and reflector savings of the 0.250 in. rod

Table 1. Critical Mass Parameters, 0.387 in. diameter Rod Lattices

$\frac{\text{Volume water}}{\text{Volume uranium}}$	% U^{235} by weight	$\frac{\text{mg } B_2O_3}{\text{ml } H_2O}$	$B^2(\text{cm}^{-2} \times 10^4)$	λ (cm)
1	1.3	0	20.90 ± 0.46	8.56 ± 0.11
	1.15	0	12.03 ± 0.91	8.60 ± 0.13
	1.0	0	3.23 ± 0.80	8.61 ± 0.16
	1.15	0.627	5.40 ± 0.89	7.99 ± 0.14
	1.15	1.119	3.64 ± 1.57	7.67 ± 0.31
1.5	1.3	0	40.51 ± 0.30	8.07 ± 0.09
	1.15	0	31.21 ± 0.35	7.81 ± 0.11
	1.0	0	19.70 ± 0.34	8.00 ± 0.12
	1.15	0.793	24.15 ± 0.90	6.54 ± 0.19
	1.15	1.493	12.87 ± 1.02	6.65 ± 0.22
2	1.15	2.93	-0.50 ± 0.54	6.03 ± 0.14
	1.3	0	52.19 ± 0.36	7.56 ± 0.08
	1.15	0	42.26 ± 0.51	7.12 ± 0.15
	1.0	0	29.02 ± 0.34	7.32 ± 0.12
	1.15	0.793	28.17 ± 1.00	6.58 ± 0.22
3	1.15	1.493	16.74 ± 0.57	6.28 ± 0.10
	1.15	3.66	-13.85 ± 0.71	5.77 ± 0.13
	1.3	0	59.25 ± 0.33	6.94 ± 0.07
	1.15	0	46.18 ± 0.37	6.81 ± 0.11
	1.0	0	31.39 ± 0.19	6.88 ± 0.12
4	1.15	0.793	26.43 ± 1.01	6.02 ± 0.18
	1.15	1.499	7.31 ± 0.54	6.15 ± 0.11
	1.15	2.247	-6.97 ± 0.67	5.78 ± 0.14
	1.3	0	54.69 ± 0.36	6.81 ± 0.08
	1.15	0	40.14 ± 0.17	6.80 ± 0.05
	1.0	0	25.68 ± 0.24	6.39 ± 0.20
	1.15	0.358	29.48 ± 0.52	6.20 ± 0.17
	1.15	0.793	15.76 ± 0.85	5.83 ± 0.21
	1.15	1.501	-9.50 ± 0.46	6.34 ± 0.11

lattices were not as accurate as was felt to be necessary. The later measurements, done with the BF_3 counters described above, are not yet all in an adequate condition to present in a formal report.

The buckling and reflector savings of twenty-nine lattices of 0.387 in. diameter rods are given in Table 1. Fourteen of these measurements were made when the moderator water contained the indicated concentrations of B_2O_3 . The other fifteen measurements were made on boron-free lattices.

Thermal Utilization

Intracell flux distributions in the 0.387 in. rods were measured with no essential changes in the techniques described in Ref. 1. Briefly, small dysprosium foils made of Dy_2O_3 embedded in polyethylene were placed in shallow holes machined in one end of a section of fuel rod, and also in a thin methyl methacrylate sheet positioned at the same height in the water. Polyethylene was used as the base for the foils rather than the methyl methacrylate reported in Ref. 1 because it seemed to have better mechanical properties. The inferred values of f are listed in Table 2.

Reference 1 contained measured values of the thermal utilization of 0.600 in. diameter rod lattices. It was at the same time pointed out that those results did not agree with similar ones obtained at Bettis, and that the difference was probably to be ascribed to the material used to hold foils in the water.

This suspicion has since been verified by measurements both at BNL and Bettis; it was found that even very thin sheets of aluminum could not correctly be used to hold the foils in the water, because of flux perturbations so introduced. This effect is caused by a mismatch of scattering cross-section between water and aluminum.

Thermal utilizations of all 0.600 in. rod lattices have been remeasured with thin methyl methacrylate foil holders, and the results are fully reported in Ref. 2.

The measurements in 0.250 in. diameter rod lattices are not yet accurate enough nor complete enough to report here.

Fast Fission Ratio

δ_{28} , the ratio of (fast) fissions in U^{238} to fissions in U^{235} , was measured in miniature lattices by the catcher foil techniques described in detail in Ref. 1. (It should be noted that the quantity F described therein is the same as the quantity now called δ_{28} .) Certain minor changes in techniques and analysis have improved the reproducibility of the results: for example, the commercial aluminum foil used for the catchers was replaced by 99.8% pure aluminum foil. The background activity was thus reduced.

Measurements of δ_{28} of 0.600 in. rod lattices have been reported in Refs. 1 and 2. The latter are an extension and improvement of the former, representing the results of repeated experiments with each of

Table 2. BNL Experimental Data, 0.387 in. Lattices

Enrich.	W/U	f	δ_{28}	δ_{21}	ρ_{28}	R_{Au}
1.0	1	0.941	0.183±0.010	0.24	2.44±0.10	1.15
	1.5	0.916	0.129±0.006	0.096	1.61±0.05	1.23
	2	0.891	0.114±0.003	—	1.35±0.05	1.31
	3	0.842	0.086±0.004	0.053	0.93±0.03	1.43
	4	0.802	0.079±0.005	0.037	0.73±0.03	1.76
1.15	1	0.945	0.177±0.005	0.22	—	—
	1.5	0.920	0.127±0.004	0.15	—	—
	2	0.898	0.108±0.002	0.10	—	—
	3	0.852	0.077±0.001	0.089	—	—
	4	0.808	0.066±0.001	—	—	—
1.3	1	0.949	0.173±0.004	0.24	—	—
	1.5	0.927	0.134±0.001	0.17	—	—
	2	0.904	0.109±0.001	0.12	—	—
	3	0.865	0.086±0.001	0.073	—	—
	4	0.823	0.073±0.001	0.052	—	—

Table 3. BNL Experimental Data 0.250 in. Lattices

Enrichment	W/U	δ_{28}	δ_{21}	ρ_{28}	R_{Au}
1.0	1.5	0.129±0.003	0.14	2.35±0.06	—
	2	0.105±0.003	0.095	2.00±0.04	1.27
	3	0.086±0.003	0.056	1.27±0.02	1.40
	4	0.063±0.002	0.050	1.02±0.01	1.59
1.15	1.5	0.136±0.002	—	—	—
	2	0.106±0.002	—	—	—
	3	0.080±0.007	—	—	—
	4	0.063±0.002	—	—	—

the fifteen lattices covered by the set of experiments. The results obtained since, with 0.387 in. and 0.250 in. diameter rod lattices, are listed in Tables 2 and 3. It may be seen that the practice of measuring the values of δ_{28} of lattices which differ only in the fuel enrichment has been continued.

U²³⁸ Cadmium Ratio

The method used to measure ρ_{28} , with application to inferring the resonance escape probability, was first published in the open literature in 1955 by Egiazarov, Dikarev, and Madeev³. Without diminishing in any degree the credit due the Soviet workers, we wish to state that the BNL group had independently developed the application of this method to ρ in 1953 and 1954. The first reliable BNL measurements on the 0.600 in. lattices were made in June 1955, too late for inclusion in the 1955 Geneva Conference. This work has been described in internal BNL memoranda, and in Ref. 2. Measurements made by the Bettis group by essentially the same methods were reported to the last Geneva Conference.⁶

The technique involves irradiating natural uranium foils of the diameter of the fuel rods between sections of fuel rod. One foil, the "bare" foil, represents a typical cross-section of fuel (if the very small effect of enrichment is neglected) and the total absorption of its U²³⁸ content is representative of that of the fuel. The other foil, together with "buttons" of fuel 0.050 in. thick, is surrounded by a Cd shield. The absorption by its U²³⁸ is representative of the epi-Cd

and fast absorption in the U²³⁸ of the fuel. The buttons ensure, by minimizing streaming paths, that the spectrum seen by the foil is typical of that seen by any section of fuel. If R_{28} is the ratio of the specific U²³⁹ activity in the bare foil to that in the Cd-covered foil, then $\rho_{28} = (R_{28} - 1)^{-1}$.

Bettis measurements⁵ of the variation of ρ_{28} with button thickness have shown that 0.050 in. is sufficient to eliminate undesirable effects of streaming through the cadmium top of the pill box.

The method, then, was to irradiate the natural uranium foils in miniature lattices, dissolve the foils in HNO₃, and chemically separate the uranium (as sodium uranyl acetate) from its daughter products and fission products. The sodium uranyl acetate was deposited as thin layers on aluminum planchets and the resulting U²³⁹ and Np²³⁹ β^- activities were measured with end-window geiger counters. In order to determine the amount of U²³⁸ in each planchet, three methods were used. First, the sodium uranyl acetate was weighed. Second, the amount of Th²³⁴ and Pa²³⁴ daughter activities were measured as they grew in. Third, the samples were chemically quantitatively analyzed for uranium. The cadmium ratios based on the three methods generally agreed to within 5%.

At the outset of these experiments, it was suspected that the cadmium pill-box enclosing the second foil might perturb the results through a local depression of the fission rate. The effect in question is of higher order, because this decrease in source strength is only felt after the neutrons have slowed down to energies where resonance capture occurs.

Estimates of the size of the perturbation indicated that if the pill-box were small enough, the effect could be neglected. This was certainly expected to be true if the height of the box were no more than one-quarter of an inch, the magnitude actually chosen. Measurements at Bettis, discussed in Ref. 5, have since confirmed this judgment. Therefore the correction to the experimental values of ρ_{28} which has been reported by Russian³ and French⁴ workers has been unnecessary.

As stated earlier, the successful use of this technique came too late to be reported at the last Geneva meeting. A complete set of values of ρ_{28} of 0.600 in. diameter rod lattices has since been reported.² Tables 2 and 3 contain measured values of ρ_{28} of 0.387 in. and 0.250 in. diameter rod lattices.

Gold Cadmium Ratio

From R_{Au} , one can estimate the relative amplitudes of the thermal and the epithermal components of the neutron flux. However, it is only the infinite dilution gold cadmium ratio which is useful in this way. Therefore in the course of measuring R_{Au} , care had to be taken to avoid the self-shielding of the gold resonance and the self-absorption of the emitted beta rays.

Measurements of R_{Au} have therefore been done in two steps. In the first, gold foils, 0.0005 in. thick, were exposed between sections of a fuel element, alternately with and without the cadmium pill-box used in measuring ρ_{28} . The second step of the measurement consisted in finding the correction which had to be made to the cadmium ratio because of the unwanted effects. This was found by exposing in the BNL Reactor Pb-Au alloy foils, 0.001–0.002 in. thick, with gold content of about one part in 10^4 , and comparing cadmium ratios with those found there with the pure gold foils.

Values of R_{Au} of 0.387 in. and 0.250 in. rod lattices are given in Tables 2 and 3.

U^{235} Fission Cadmium Ratio

The techniques used to measure δ_{28} and ρ_{28} were combined in the measurement of δ_{25} . The methods have been described in Ref. 2, which contains the experimental results for lattices of 0.600 in. rods. Tables 2 and 3 list experimental values of δ_{25} for 0.387 in. and 0.250 in. diameter rod lattices.

The catcher foils used to measure the fission rates receive fission products also from U^{238} . This has been a severe perturbation to the epithermal catcher activity, amounting to as much as ninety per cent of the observed count rate. The corrections needed to eliminate this unwanted effect were therefore quite large, and so the experimental values show considerable scatter. The measurements will be repeated in the near future by the more precise methods used at Bettis and described later.

Neutron Temperature of Moderator

The effective temperatures of low energy neutrons

in the moderator of five lattices of 0.387 in., 1.3% and 1.15% enriched rods have been measured. The method has been described to the last Geneva conference.¹ The precise techniques used for these more recent measurements differ from those reported earlier, and so we will discuss this measurement in some detail.

The addition of a small amount of neutron poison to the moderator of a multiplying system causes a small change in reactivity. The quantity $d\rho/dn$, which is the reactivity change per unit atom density of the poison, is proportional to the absorption cross-section of the poison, averaged over the energy distribution of the neutrons. If the low energy distribution can be represented as approximately Maxwellian, it can be characterized by a value of the neutron temperature. The danger coefficient $d\rho/dn$ is therefore a function of the neutron temperature.

The measurement based on these considerations was done as follows. Separate solutions of H_3BO_3 and $CdSO_4$ of known molar concentrations were prepared. Accurately measured quantities of each were successively added to the moderator water of the lattice being studied, and the changes in reactor period were measured. From these were deduced the value:

$$\left(\frac{d\rho}{dn}\right)_B / \left(\frac{d\rho}{dn}\right)_{Ca}$$

This quantity was also calculated as a function of the neutron temperature, under the assumption that the energy distribution of the neutrons was precisely Maxwellian. The measured ratio in each case then corresponded to a unique neutron temperature. Values deduced in this way are listed in Table 4 for the five lattices of 0.387 in. diameter rods with which the measurement was performed. The result for the 0.600 in. lattice in Table 5 was done in a subcritical lattice by neutron multiplication methods and was previously reported in Ref. 1.

Table 4. Effective Neutron Temperatures
(Moderator temperature: 209°K)

Rod diam.	Enrichment	W/U	$\bar{\sigma}_{Ca}/\bar{\sigma}_B$	$\theta_m(^{\circ}K)$
0.387 in.	1.3%	2	4.94	321 ± 30
0.387 in.	1.3%	3	5.03	329 ± 30
0.387 in.	1.3%	4	5.21	343 ± 30
0.387 in.	1.15%	3	4.63	294 ± 25
0.387 in.	1.15%	4	4.62	293 ± 15
0.600 in.	1.15%	3	4.72	297 ± 16

Table 5. Summary of Lattices Studied at Bettis

	Enrichment	Fuel diameter, inches	W/U
Uranium metal ^a	1.3%	0.600	1.5, 2, 3
Uranium metal	1.3%	0.387	2, 3
Uranium metal	1.15%	0.600	2, 3
UO ₂ (7.53 gm/cm ³)	1.3%	0.601	3, 4, 5
UO ₂ (7.52 gm/cm ³)	1.3%	0.388	4, 5
UO ₂ (10.53 gm/cm ³)	1.3%	0.383	3, 3.6, 5

^a These lattices were reported in Ref. (6). Because the data were given in a different manner, they are included here for completeness.

It should be pointed out that the difference in character between the actual neutron spectrum and the assumed Maxwell form adds a degree of uncertainty to the measurement. An improved interpretation can be made based on the assumption that the spectrum is Maxwellian with a 1/E tail or is of the Wigner-Wilkins form. This improvement has not been made here.

Bettis Experiments

Description of the Facility and Assemblies

The experimental data at Bettis on light water moderated, slightly enriched uranium and uranium oxide rod lattices have been obtained by critical assembly techniques. The critical facility, known as the TRX, has been described previously,^{5,6} and only its major features will be repeated here. The lattices for which data have been obtained are listed in Table 5, with the lattice geometry given in Appendix 1.

All the lattices contained cylindrical fuel rods of 48 in. length, sheathed in aluminum tubing of 0.028 in. wall thickness. The UO₂ fuel was in the form of short cylindrical pellets stacked to give the 48 in. fuel height. The critical assemblies have been designed to provide data under those conditions most conducive to theoretical analysis. To meet this objective, the following features of the lattices are important :

- (a) The basic lattice cell was an equilateral triangle (hexagonal array).
- (b) The critical assemblies were built to approximate right circular cylinders.
- (c) The control elements fitted between the fuel rods, so that when they were withdrawn, the water to uranium metal ratio was uniform throughout the core.

The volume ratio of water to uranium metal

(W/U) is the parameter used to specify the fuel spacing. The term as applied to uranium metal lattices is self-explanatory. As used to refer to uranium oxide fueled systems, however, it must be defined carefully. If the water to UO₂ volume ratio is designated as (W/UO₂), the corresponding value of (W/U) is defined as that of the metal lattice which has the same H/U atom ratio, thus :

$$\left(\frac{W}{U}\right) = \frac{m_U}{m_{UO_2}} \frac{M^{UO_2}}{M^U} \left(\frac{W}{UO_2}\right)$$

where *m* and *M* are the density and the molecular weight of the indicated materials.

Intensive Parameters

Measurements of *f*, δ₂₈, and ρ₂₈ were made with the 1.3% enriched uranium metal and uranium oxide fueled lattices. The experimental techniques and the results have been published elsewhere,⁵ but for completeness the results are also presented in Table 6.

The quantity δ₂₅, defined earlier as the number of epi-cadmium fissions in U²³⁵ per sub-cadmium fission in U²³⁵, has also been measured, but not previously reported. The following technique was used. Two foils, each containing ten weight per cent of highly enriched uranium in aluminum, were used. These were irradiated, one bare and one cadmium encased, between segments of a fuel rod in the core of the critical assembly. The gamma radiation induced in each was measured at the same time after shutdown with a sodium iodide scintillation counter biased to reject pulses corresponding to gamma rays below 400 kev. The results are listed in Table 6.

The earliest measurements made use of a cadmium pill-box similar to that used in the measurement of ρ₂₈. It was, however, found later that the 0.015 in.

Table 6. Bettis Experimental Data

Rod diam. (inches)	Fuel	Enrichment %	W/U	W/UO ₂	($\bar{\phi}_m \bar{\phi}_u$)	<i>f</i>	ρ ₂₈	δ ₂₈	δ ₂₅	C.R.
0.600	Metal	1.3	1.5	—	1.39±0.04	0.918±0.004	1.80±0.18	—	—	—
0.600	Metal	1.3	2.0	—	1.45±0.04	0.890±0.004	1.24±0.12	—	—	—
0.600	Metal	1.3	3.0	—	1.49±0.04	0.843±0.003	0.89±0.09	—	—	—
0.600	Metal	1.15	2.0	—	1.45±0.04	0.881±0.004	1.20±0.03	0.104±0.015	—	—
0.600	Metal	1.15	3.0	—	1.45±0.04	0.835±0.005	0.93±0.04	0.081±0.012	—	—
0.387	Metal	1.3	2.0	—	1.21±0.04	0.904±0.003	1.59±0.03	0.099±0.015	0.150±0.010	0.68±0.01
0.387	Metal	1.3	2.4	—	1.24±0.02	0.889±0.003	1.39±0.03	0.103±0.005	0.104±0.004	0.66±0.01
0.387	Metal	1.3	3.0	—	1.31±0.04	0.857±0.004	1.18±0.03	0.078±0.012	0.099±0.003	0.60±0.01
0.600	UO ₂ (7.53 g/cm ³)	1.3	3.0	1.07	1.09±0.03	0.873±0.004	1.19±0.04	0.071±0.010	0.080±0.003	0.62±0.01
0.600	UO ₂ (7.53 g/cm ³)	1.3	4.0	1.40	1.14±0.03	0.837±0.005	0.994±0.013	0.059±0.009	0.077±0.002	0.56±0.01
0.600	UO ₂ (7.53 g/cm ³)	1.3	5.0	1.76	1.16±0.03	0.805±0.005	0.807±0.014	0.051±0.004	0.072±0.002	0.51±0.01
0.388	UO ₂ (7.52 g/cm ³)	1.3	4.0	1.39	1.10±0.01	0.836±0.004	1.04±0.05	0.063±0.003	0.078±0.002	0.58±0.01
0.388	UO ₂ (7.52 g/cm ³)	1.3	5.0	1.73	1.10±0.01	0.807±0.004	0.901±0.02	0.054±0.003	0.063±0.002	0.55±0.01
0.383	UO ₂ (10.53 g/cm ³)	1.3	2.9	1.42	1.10±0.01	0.874±0.004	1.43±0.01	0.078±0.004	0.089±0.002	0.68±0.01
0.383	UO ₂ (10.53 g/cm ³)	1.3	3.6	1.78	1.13±0.01	0.848±0.004	1.15±0.01	0.070±0.004	0.072±0.001	0.61±0.01
0.383	UO ₂ (10.53 g/cm ³)	1.3	4.9	2.40	1.13±0.01	0.809±0.004	0.934±0.01	0.057±0.003	0.055±0.001	0.56±0.01

cadmium wall allowed the transmission of 0.5% of the thermal neutrons. Since the cadmium ratios were in the neighborhood of 10, there were associated errors of approximately 5% in the activation of the cadmium covered foils. When the measurement was made in oxide fuel, it was also found necessary to exclude the oxide spacer which was needed in the measurement of ρ_{28} . This spacer, situated between the detecting foil and the cadmium wafer, tended to moderate the epi-cadmium neutrons after their transmission through the cadmium. Both of these effects make the reported values of δ_{25} too large. The quoted uncertainties in δ_{25} therefore reflect these errors. Later measurements have been made with 0.820 in. cadmium and no fuel spacers.

The last column in Table 6 lists the conversion ratios of the lattices studied. The conversion ratio can be expressed in terms of the other parameters in Table 6, and so required no additional experiments. Values were calculated from the expression

$$CR = \frac{\sum_{a_{th}}^{28} (\rho_{28} + 1)}{\sum_{a_{th}}^{25} \left[1 + \delta_{25} \frac{(1 + \bar{\alpha}_e^{25})}{(1 + \bar{\alpha}_{th}^{25})} \right]}$$

where $\sum_{a_{th}}$ is the thermal absorption cross section, $\bar{\alpha}_e^{25}$ is the ratio of the average capture to fission in U^{235} in the epi-cadmium region, and $\bar{\alpha}_{th}^{25}$ is the same quantity in the thermal region. The values of $\sum_{a_{th}}$ were taken from BNL-325 and the values of $\bar{\alpha}_e^{25}$ and $\bar{\alpha}_{th}^{25}$ were assumed to be 0.4 and 0.18 respectively.

Buckling and Reflector Savings: Introduction

Bettis measurements of extensive core parameters have not been reported before, and so will be described here in some detail.

In preparation for a measurement, the lattice concerned was built up to critical size in steps, with the final critical configuration (actually one giving a slightly positive period) arranged to provide as nearly a cylindrical boundary as possible. Although the boundary could not be truly cylindrical, the approximation to a cylinder was always quite good. The radius R of the equivalent cylindrical lattice containing N fuel rods was defined in terms of the unit cell r_e radius as:

$$R = r_e N^{\dagger} \quad (1)$$

Values of r_e are listed in Appendix 1.

The neutron flux in the central region of a critical lattice which is large compared to a neutron migration length can be separated into radial and axial functions which are independent of neutron energy and which are characteristic of the radial and axial geometrical bucklings. In this region we have (as in a bare core):

$$\text{Flux} = A J_0(B_r r) \cos(B_z z) \quad (2)$$

where r and z are measured from the center of the

lattice, and the geometrical buckling is:

$$B_g^2 = B_r^2 + B_z^2 = \left(\frac{2.405}{R_e} \right)^2 + \left(\frac{\pi}{H_e} \right)^2 \quad (3)$$

R_e and $H_e/2$ are the values of r and z , respectively, at which the radial or axial flux extrapolates to zero. Thus, R_e and H_e are the equivalent bare core dimensions. From the physical size of the core, R and H , we define reflector savings as usual:

$$\begin{aligned} R_e &= R + \lambda_r \text{ with } \lambda_r \text{ the radial reflector savings.} \\ H_e &= H + \lambda_z \text{ with } \lambda_z \text{ the total axial reflector savings.} \\ &\quad \text{(top and bottom)} \end{aligned}$$

$$\text{Thus: } B_r^2 = \left(\frac{2.405}{r_e N^{\dagger} + \lambda_r} \right)^2; \quad B_z^2 = \left(\frac{\pi}{H + \lambda_z} \right)^2 \quad (4)$$

The independence of flux distribution and energy in the asymptotic region, an experimental proof of which is given later, suggests that flux plots can be obtained by measurement of an activity induced by neutrons of many energies. It can be shown that activities measured in successive volumes along a traverse in this asymptotic region can be interpreted as though they were measured at equivalent points in the volumes. No correction is required for the finite size of an activated foil. In addition, flux plots may be obtained from fission product activity induced in the fuel rods themselves.

Flux distributions have been measured by two methods. The first of these used uranium metal foils exposed in the fuel rods. The foils consisted of 1.3% enriched uranium metal 0.005 in. thick and of diameter equal to that of the fuel in the lattice under investigation. Each foil was placed in a composite formed of a short section of fuel, a 0.002 in. thick aluminum spacer, the uranium foil, another aluminum spacer, and another section of fuel. This composite was taped together with a single thickness of 0.001 in. Mylar tape and assembled with other composites or sections of fuel into a fuel rod.

The second method involved measuring the induced fission product activity in the fuel rods themselves. This rod counting technique was used more often than the other, since it eliminated the loading and unloading of foils. Where foils were used in the axial flux measurements, the rod technique was checked against the foil technique, and a similar check on the radial plots was occasionally performed. Within experimental error, the two always gave the same results.

The number of fuel rods in the core was chosen so that upon withdrawal of all control elements, the neutron flux level increased exponentially with a period of, for example, 300 sec. When the flux reached a predetermined level, all control rods were quickly dropped into the core. The exposure over the last two decades of the rise was of the order of 20 min.

The gamma activity from the irradiated foils or fuel rods was measured with scintillation counters each of which consisted of a 2 in. thick NaI crystal

Table 7. Results of Bettis Buckling and Reflector Savings Measurements

Lattice designation		Critical no. of fuel rods at 20°C	Critical buckling (20°C) (cm ⁻²) × 10 ⁴	Radial reflector savings cm	Total axial reflector savings cm
Fuel	W/U				
U metal	2	904 ± 2	53.55 ± 0.48	7.40(2) ^a ± 0.17	14.07 (1) ^a ± 0.71
1.3%, 0.387 in.	3	630 ± 2	58.2 ± 1.00	7.22(1) ± 0.31	14.23 (1) ± 0.82
UO ₂ , 7.53 gm/cm ³	3	1269 ± 3	28.37 ± 0.06	8.55(5) ± 0.06	17.82 (5) ± 0.23
1.3%, 0.601 in.	4	1027 ± 3	30.17 ± 0.06	8.36(4) ± 0.06	16.72 (4) ± 0.19
	5	987 ± 3	29.06 ± 0.07	7.92(4) ± 0.07	15.90 (5) ± 0.22
UO ₂ , 7.52 gm/cm ³	4	3045 ± 3	25.28 ± 0.10	8.41(4) ± 0.12	17.06 (6) ± 0.51
1.3%, 0.388 in.	5	2784 ± 3	25.21 ± 0.10	8.08(4) ± 0.12	15.37 (3) ± 0.26
UO ₂ , 10.53 gm/cm ³	3	2173 ± 3	32.59 ± 0.15	7.86(6) ± 0.12	15.27(11) ± 0.41
1.3%, 0.383 in.	3.6	1755 ± 3	35.47 ± 0.18	7.41(5) ± 0.13	14.69 (8) ± 0.43
	5	1575 ± 3	34.22 ± 0.13	7.10(7) ± 0.10	14.52 (8) ± 0.17

^a Number of measurements indicated in parentheses.

on a 5819 photomultiplier. Gamma activity from an irradiated fuel rod was detected by a horizontal scintillation head which viewed the vertical fuel rod through a collimator. In the course of counting an axial traverse, a single fuel rod was moved in successive steps along its own axis past the collimator. In counting a radial traverse, the same axial positions of a number of fuel rods were successively exposed before the collimator. During counting, the pulse height discriminators were always set to reject pulses below 400 kev.

The values of the relative measured activity within the asymptotic region of each traverse were fitted by a least squares iteration technique to the appropriate function. In the fitting process, only the experimental points within the asymptotic region of flux separability could be used. If points too near the reflector were used, the fitted function would be in error and if too few points were used, the error in the inferred buckling became large.

Most of the measured flux plots extended to the boundaries. Care was taken in the analysis, therefore, to determine the extent of the core over which the assumption of an asymptotic behavior was reliable. A sufficient number of cases have been investigated to establish a general criterion for the extent of this asymptotic region in the lattices studied here. The asymptotic core volume extended from the core center to the following approximate limits: 70% in an axial direction and 55% in a radial direction of the distances to the extrapolated zeros of $\cos [B_z(z-z_0)]$ and $J_0(B_r r)$, respectively.

The buckling as obtained from a least squares fit to flux distributions in a critical assembly is not the critical buckling, since measurements are always taken with a slight excess reactivity. The excess reactivity during measurements reported here varied slightly from one instance to another, because of temperature changes and differences in fuel rod loading. The reflector savings inferred from the buckling determinations did not however vary in this way. Thus, the reflector savings was averaged and not the buckling itself.

The value of the critical buckling was calculated from this average reflector savings and the number

of fuel rods required for criticality. The geometrical buckling at any fuel rod loading could be calculated through use of this same reflector savings.

The critical number of fuel rods at 20°C, the axial and radial reflector savings, and the critical buckling at 20°C are listed in Table 7. The critical number of fuel rods at 20°C was obtained from short extrapolations of data taken near 20°C during temperature coefficient measurements. The average value of reflector savings and the quoted error were obtained by using as weight functions the inverse squares of the errors obtained from the standard deviations of the individual measurements. The variation in the number of rods listed in Table 7 is due principally to reproducibility errors. The error on the buckling is a direct reflection of the uncertainty in the number of fuel rods and the error in the reflector savings.

Results of Special Measurements

To check two hypotheses used earlier, that the flux of all neutron energies had the same buckling, and that the radial reflector savings did not depend upon the radius, the following two experiments were performed:

1. Radial flux traverses were taken in two lattices with uranium metal foils highly depleted in U²³⁵ (5 ppm U²³⁵). These foils were counted in the same way as the regular foils described earlier, except that the discriminator bias was set at 1.2 Mev to eliminate bremsstrahlung from the 1.2 Mev γ -ray of U²³⁹. Thus these foil activities represented the distribution of neutrons above the U²³⁸ fission threshold at about 1 Mev. Reflector savings were obtained by least squares fitting, and the results were compared with the reflector savings obtained from the predominantly thermal neutron distribution found with the usual 1.3% enriched foils.

Table 8. Radial Reflector Savings (cm) from Fast Flux Plots

	Using depleted foils	Using 1.3% enriched foils
Lattice I	7.63 ± 0.17	7.40 ± 0.17
Lattice II	7.41 ± 0.14	7.22 ± 0.31

The results in Table 8 indicate that within experimental error the reflector savings, and hence the buckling, were energy independent.

- Measurements were made at two different loaded radii of each of two lattices to test the assumption that radial reflector savings was not a function of the loaded radius. This assumption is important later. In performing the measurement, a larger radius was obtained by adding fuel rods to the periphery of the core while maintaining the approximately cylindrical shape. To retain criticality, the water height was reduced. Radial flux plots were measured with all control rods removed. The results (in Table 9) indicate that the assumption tested was valid within the experimental error of the measurement. It should also be noted that the same assumption has been found to be true in the exponential experiments at BNL where even much smaller radii than those used here were involved.¹

Table 9. Independence of Radial Reflector Savings with Respect to Radius

	Radius (cm)	Reflector savings (cm)
Lattice I	39.70	8.36 (4) \pm 0.06
	48.22	8.35(2) \pm 0.20
Lattice II	38.12	7.86 (6) \pm 0.12
	42.60	8.01 (2) \pm 0.35

^a Number of measurements indicated in parenthesis.

The independence of reflector savings with respect to assembly temperature over the interval between 20°C and 50°C has also been assumed in some of the later analyses. This assumption has been checked over a smaller temperature range. Individual flux plots measured at temperature differences of as much as 15°C showed within experimental error no change in reflector savings. The assumption has not been tested over the complete temperature range of interest but it did appear to be valid within the error quoted for reflector savings.

The assumption of separability of radial and axial fluxes within the asymptotic region has also been verified by comparing axial flux traverses taken at different distances from the center of the lattice. Within the assumed asymptotic region these flux traverses gave the same value for the axial buckling as those taken at the center. Similar experiments with radial plots at several values of z were performed with the same result.

Temperature Coefficient of Reactivity

Measurements of the reactivity change associated with a given temperature change were made at several temperatures of each lattice.

The method involved finding the reactor period at each of two stable temperatures, θ_1 and θ_2 , with the fuel rod loading being kept fixed. The difference between θ_1 and θ_2 was usually about 5°C and the corresponding periods were in the neighborhood of

100 sec and 1000 sec. The periods were converted to reactivity by means of the inhour equation in Appendix 2 and the temperature coefficient at the average of the two temperatures was found as the reactivity difference divided by the temperature difference. This designation as the coefficient at the average temperature is valid if the temperature coefficient is linear with temperature. This was the case for all the lattices studied (see below).

Measuring the coefficient at a different temperature required changing the fuel rod loading. The coefficient was then found at the new average temperature, and a plot of temperature coefficient vs temperature was so developed. Such plots were found within the experimental errors to be linear with temperature. Therefore it was justifiable to fit data for each lattice to a straight line by a least squares procedure in which each point was weighted inversely as the square of its error.

From such weighted least squares fits, the temperature coefficients of each lattice at 20°C and at 40°C were obtained. The results are listed in Table 10, with the number of points used in the least squares fits shown in parentheses. The error quoted was determined from the standard deviation of the residuals in the least squares analysis. It can be seen that the temperature coefficient was negative at 20°C for nearly all the lattices and became more negative as the temperature was increased. These results are valid only to about 50°C since no measurements were made much above that temperature.

Table 10. Temperature Coefficient Results

Lattice designation Fuel	W/U	$\frac{d\rho}{d\theta}(\text{°C}^{-1}) \times 10^4$	
		20°C	40°C
U metal 1.3%, 0.600 in.	2	-0.36(2) \pm 0.02	-0.76 \pm 0.02
	3	+0.10(6) \pm 0.02	-0.19 \pm 0.02
U metal 1.15%, 0.600 in.	2	-0.40(12) \pm 0.02	-0.74 \pm 0.02
	3	+0.11(4) \pm 0.02	-0.14 \pm 0.02
U metal 1.3%, 0.387 in.	2	-0.46(8) \pm 0.04	-0.82 \pm 0.04
	3	-0.47(6) \pm 0.02	-0.78 \pm 0.02
UO ₂ , 7.53 gm/cm ³ 1.3%, 0.601 in.	3	-0.71(10) \pm 0.02	-0.93 \pm 0.02
	4	-0.66(6) \pm 0.02	-0.87 \pm 0.02
	5	-0.55(6) \pm 0.02	-0.83 \pm 0.02
UO ₂ , 7.52 gm/cm ³ 1.3%, 0.388 in.	4	-0.85(5) \pm 0.02	-1.02 \pm 0.02
	5	-0.90(4) \pm 0.03	-1.01 \pm 0.03
UO ₂ , 10.53 gm/cm ³ 1.3%, 0.383 in.	3	-0.57(27) \pm 0.07	-0.89 \pm 0.07
	3.6	-0.69(38) \pm 0.05	-0.87 \pm 0.05
	5	-0.72(10) \pm 0.02	-0.87 \pm 0.02

^a Number of measurements used in the least squares fits is indicated in parentheses.

Buckling Coefficient of Reactivity

The reactivity of any given lattice of fixed composition can be changed by altering the temperature or the size of the lattice or both. The previous section discussed reactivity changes which occurred when the temperature was varied, while the number of

fuel rods remained constant. This section treats the reactivity changes accompanying a size change, while the temperature remains fixed. These data are of use in estimating the migration area.

The size change was accomplished by adjusting the height of the water in the lattice or by adding or removing fuel rods from the cylindrical periphery. B_g^2 and its changes were calculated by use of the expression given earlier.

The experiments to be described measured the first derivative of reactivity with respect to geometrical buckling. Both methods mentioned above were used to obtain $d\rho/dB_g^2$; one from changes in radial buckling at constant axial buckling and the other from changes in axial buckling at constant radial buckling.

$d\rho/dB_g^2$ from Changes in Radial Buckling

Altering the radial buckling over a wide range introduced large reactivities which had to be compensated by making some other reactivity change. The other variable used in these experiments was the temperature, which was changed occasionally to keep reactivities reasonably near to critical. Thus, the set of data obtained consisted of values of reactivity at various lattice sizes and various temperatures.

The method devised simultaneously provided data for finding $d\rho/dB_g^2$ and the temperature coefficient. Groups of up to four fuel rods from as many as six places around the periphery of a lattice were remotely removed from and reinserted into the lattice. The number of fuel rods in the lattice, including the ones which could be later removed, was initially adjusted to give a reactor period of perhaps 80 seconds (reactivity of $\sim 10 \times 10^{-4}$) at the initial temperature. At this temperature, values of reactivity were measured at the full number of fuel rods, when one group of four fuel rods was removed, when another group was removed, and so forth until the reactivity was nearly zero. The fuel rods were then reinserted, the temperature raised perhaps 5°C, and reactivities again measured as the various groups of fuel rods were removed. If sufficient reactivity remained, another temperature change was made. An advantage of the method is that considerable data were obtained without altering the reactor conditions by dumping the water, making fuel rod changes, and starting up again.

Studies using this remote fuel rod pulling technique indicated that within experimental error the reactivities observed depended on the numbers of fuel rods loaded, but not on their specific geometry. That is, a lattice with two groups of rods removed had the same reactivity whether these two groups were adjacent or on opposite sides of the lattice. This was apparently only because of the large number of fuel rods (between 1000 and 3000 for the UO₂ lattices), so that slight irregularities on the boundary averaged out.

After the radial buckling at each of the lattice loadings was calculated, the data obtained were

plotted as a graph of reactivity vs radial buckling at each of the temperatures. The axial buckling was constant at all loadings of a given lattice, so that $d\rho/dB_g^2 = d\rho/dB_r^2$. Thus, the measurements of reactivity made at a given temperature with the various fuel rod groups successively removed formed a curve whose slope was the same as that of reactivity vs. buckling for that temperature. The striking feature of these curves is that they were all straight lines over the range of reactivities used. Therefore the data at each temperature were fitted by least squares to straight lines and values of $d\rho/dB_r^2$ at each temperature were obtained along with the errors in these quantities. The buckling obtained by extrapolating the straight line at each temperature to zero reactivity was the critical radial buckling at that temperature.

Table 11. $d\rho/dB_g^2$ at Full Water Height and at Partial Water Height^a

Lattice designation Fuel	W/U	$d\rho/dB_r^2$ cm ²	$d\rho/dB_z^2$ cm ²	λ_z cm
U metal 1.3%, 0.600 in.	2	-28.2 (1) ^b		
U metal 1.15%, 0.600 in.	2	-26.9 (4)		
U metal 1.3%, 0.387 in.	2	-29.0 (3)		
	3	-29.9 (4)		
UO ₂ , 7.53 gm/cm ³ 1.3%, 0.601 in.	3	-46.1 (7)	-50.4	19.02 ± 0.29
	4	-44.9 (4)	-47.5	17.66 ± 0.19
	5	-41.1 (4)		
UO ₂ , 7.52 gm/cm ³ 1.3%, 0.388 in.	4	-47.3 (4)		
	5	-48.2 (3)		
UO ₂ , 10.53 gm/cm ³ 1.3%, 0.383 in.	3	-39.1 (10)	-43.0	17.11 ± 0.22
	3.6	-38.6 (23)	-39.4	15.82 ± 0.41
	5	-35.4 (8)	-37.3	15.51 ± 0.21

^a See text for accuracy.

^b Number of measurements at all temperatures.

Table 11 summarizes the results. Since the data from individual measurements at various temperatures had too much dispersion to provide any variation with temperature, the values listed in Table 11 are average values at all temperatures, with each determination weighted inversely as the square of its error. An error of $\pm 5\%$ has been assigned the final average value; this is believed to be conservative. In taking this average, the assumption was therefore made that $d\rho/dB_r^2$ is not a function of temperature. This assumption is neither contradicted nor reinforced by the data but appears appropriate within the error assigned to the average.

$d\rho/dB_g^2$ from Changes in Axial Buckling

The other method to determine the change in reactivity with buckling varied the axial buckling while the radial buckling remained fixed. The method, which is often referred to as the partial water height measurement, proceeded as follows:

The lattice was made critical with the water at

some height h_c less than the full fuel height. The radial buckling was estimated from the number of loaded fuel rods and the previously measured radial reflector savings. Several different fuel loadings were used in the course of measurements on any single lattice, to provide two or three critical water heights in the range from 24 in. to 40 in.

A partial water height axial reflector savings λ_z' was then obtained from measured flux plots. The value of B_z^2 for any water height near the critical level was calculated from the relation:

$$B_z^2 = \left(\frac{\pi}{h + \lambda_z'} \right)^2 \quad (5)$$

with a fixed λ_z' .

The critical height, h_c , of the water was measured as that height which gave an infinite reactor period. h_c was measured by means of a probe which made electrical contact with the water surface, giving the critical height to within about ± 0.1 in. absolutely and within about ± 0.005 in. relative to any other measured height.

After the reflector savings and critical height were measured, the reactivity was determined at each of two heights h_1 and h_2 above the critical height, the larger of these generally being about 0.5 in. above the critical value. The difference in axial buckling was then found from:

$$\Delta B_z^2 = -\pi^2 \frac{(h_1 + h_2 + 2\lambda_z')\Delta h}{(h_1 + \lambda_z')^2 (h_2 + \lambda_z')^2} \quad (6)$$

To improve the accuracy in Δh and so in turn reduce the error in ΔB_z^2 , it was necessary to devise a more accurate measuring system. The procedure adopted was based on accurate weighing of the amount of water constituting the height difference Δh . The height change was thus determined to within ± 0.001 in.

The value of ΔB_z^2 could then be calculated. The values of λ_z' measured and used are also listed in Table 11. It is to be noted that the axial reflector savings did vary with critical water height, in a manner which might qualitatively be explained by the assumption that the varying thickness of dry uranium lattice above the water surface was effectively approaching an infinite value.

The values of $d\rho/dB_z^2$ obtained are also listed in Table 11. There was an evident trend with any given lattice toward larger negative values of $d\rho/dB_z^2$ as the water height was lowered, in a direction consistent with the above effect. It was assumed earlier in this paper that the axial reflector savings is constant at

heights near the critical height. This assumption was apparently not valid when there was less than 30 cm of dry lattice above the water surface.

For these reasons, the only measurements of $d\rho/dB_z^2$ that should be considered as approximating the correct values are those from measurements at heights less than 36 in. (92 cm). Only the numbers which meet this criterion are reported in Table 11.

Slightly Enriched Pu Lattices

A set of measurements was made at BNL on lattices whose fuel was 1% Pu, 0.3% U²³⁵, 98.7% U²³⁸. The rods were 0.387 in. in diameter, 4 ft long, and were clad like the slightly-enriched uranium lattices reported above. A small number (37) of these rods formed a central sub-lattice in a larger lattice made up of 1.3% enriched uranium rods, and the critical radius of such a two-region lattice was determined by sub-critical multiplication methods and compared with that of a uniform lattice containing only the uranium. These measurements were done at water to uranium volume ratios of 2, 3, and 4.

The buckling of the Pu region was obtained by a one-group, two region analysis.

The bucklings were then calculated by the Yankee Electric Project group from the four factor formula.⁸ ϵ was calculated from an empirical formula based on the uranium lattice measurements. p was obtained from an assumed form of the resonance integral of U²³⁸, including the "Dancoff correction" for shielding of the surface absorption by neighboring fuel rods. ηf was calculated from cross-sections. τ was calculated from one velocity fast neutron removal and transport cross sections which were themselves obtained from fits to experimental data on various materials. L^2 was calculated from flux-weighted diffusion coefficients and absorption cross sections. It was assumed in all these calculations that the Pu contained 1% Pu²⁴⁰, 99% Pu²³⁹.

Table 12 lists the calculated values of ϵ , p , ηf , τ , L^2 and B^2 , and the values of the buckling inferred from the measurements, B_m^2 , for each of the lattices.

The two-region analysis is expected to be reasonably valid when the two regions have bucklings that are not too different, and their diffusion coefficients are the same. Previous experiments at BNL on lattices in which the two regions were of different enrichments of uranium had given results for the "unknown" buckling which were correct. It is questionable whether the Pu region fulfills the above requirements closely enough; furthermore a number of uncertainties entered into the calculations. The

Table 12. Constants of Pu-Enriched Lattices

W/U	ϵ	p	ηf	k_∞	$\tau(\text{cm}^2)$	$L^2(\text{cm}^2)$	$B^2(\text{m}^{-2})$	$B_m^2(\text{m}^{-2})$
2	1.0581	0.7787	1.646	1.356	44.8	0.964	77.4	76.8
3	1.0448	0.8423	1.595	1.404	40.7	1.225	95.2	92.6
4	1.0363	0.8775	1.540	1.400	38.5	1.474	98.8	93.1

agreement between the calculated bucklings and those inferred from the two-region measurements must therefore be regarded as fortuitous to some extent, and the results are reported here only because no other results of this type on uranium systems containing Pu have been published.

Inferences from the Existence of a Simple Critical Equation

The multigroup methods of analysis discussed later do not lead to a critical equation form for the neutron leakage probability. Instead, this probability is calculated separately for each energy group. Since there is cross-linkage of a complicated nature between groups, the overall non-leakage probability is not a simple product of the different group values. The few group treatments which have been developed from the multigroup theory do lead to reasonably simple critical equations. These developments are quite recent. Their initial application to analysis of the neutron leakage indicates that the classical expressions, in which k_{eff} is equal to k_{∞} times a non-leakage probability, are not strictly valid when applied to reactor cores of this kind. The reason for this result is the large epi-thermal fission rates which supplement the thermal ones and which lead to alternatives to fission by thermal neutrons.

The application of the few group treatments to analysis of the large body of experimental data has only begun, so complete results cannot yet be reported. The only complete analysis of experimental searches for neutron leakage and migration areas which can be presented here is that which uses one of the classical forms coupled with traditional approximations. There are good grounds for altering the critical equation, and the associated migration area will also be changed. The predicted values of k_{∞} and the reactivity which would be calculated in a given physical situation would however not change very much.

For simplicity, the one group critical equation will be used here.

Migration Area, BNL Exponential Experiments

Values of the migration area of 0.387 in. diameter metal rod lattices have been deduced from the experimental data presented earlier. The basis of the analysis has been described fully in Refs. 1 and 2. As discussed there, the method depends on the change in buckling associated with poisoning the moderator water and also that caused by changing the fuel enrichment at a fixed rod spacing. The values of B^2 used are those in Table 1. The values of f for clean (unpoisoned) lattices were taken to be those of Table 2. In finding the thermal utilization of boron poisoned lattices, it was assumed that the small amounts of additional absorption in the moderator do not change the intracell flux distributions. Therefore the same disadvantage factors were used for these as for the corresponding clean lattices. The moderator absorp-

tion cross-sections were calculated from the data of BNL-325 and from the boron concentrations at which measurements of B^2 were made.

As was done with the 0.600 in. diameter rod lattice data, M^2 was found separately from the variation of B^2 and f with poison content and also from their dependence on fuel enrichment. All data were then combined, and the migration areas implied by the mutual dependence of f and B^2 were calculated.

Table 13. Migration Areas, 0.387 in. Lattices (BNL)

W/U	M^2 (cm ²)
1	39.5 ± 1.9
1.5	39.9 ± 1.4
2	35.7 ± 0.8
3	35.2 ± 1.2
4	34.0 ± 1.4

The results of the one-group analysis are listed in Table 13. The errors are based on the standard deviations of the least squares fitting. A check against the 0.600 in. diameter rod lattice results shows that the new values are noticeably larger. Most if not all of the difference must however be attributed to the greater fraction of aluminum and void surrounding the smaller rods.

Anisotropy of Migration Area

Before presenting the analysis of the migration area based on measurements at Bettis, it is necessary to deal with another measurement carried out at the same laboratory. This is an evaluation of the anisotropy of the migration area.

The anisotropy was inferred from the measurements of the critical buckling at different height-to-diameter ratios of the lattices. The one-group form of the critical equation of a cylindrical reactor which allows for anisotropy is

$$k_{\infty} = 1 + M_z^2 B_{zc}^2 + M_r^2 B_{rc}^2 \quad (7)$$

Here, k_{∞} represents the infinite medium multiplication factor, M_z^2 and M_r^2 represent effective migration areas in axial and radial directions, and B_{zc}^2 and B_{rc}^2 represent critical axial and radial bucklings. If the radius and height of the reactor are both changed so as to maintain criticality, the critical axial and radial bucklings may be measured before (B_{zc1}^2 , B_{rc1}^2) and after (B_{zc2}^2 , B_{rc2}^2) the change. Other parameters in Eq. (10) remain fixed during the change, thus:

$$M_z^2 B_{zc1}^2 + M_r^2 B_{rc1}^2 = M_z^2 B_{zc2}^2 + M_r^2 B_{rc2}^2 \quad (8)$$

The anisotropy ratio, A , is here defined as the ratio M_z^2/M_r^2 . Eq. (8) may be rearranged to yield:

$$A = \frac{B_{rc2}^2 - B_{rc1}^2}{B_{zc1}^2 - B_{zc2}^2} = - \frac{\Delta B_{rc}^2}{\Delta B_{zc}^2} \quad (9)$$

From the critical axial and radial bucklings determined from measured reflector savings at various partial water heights and at full water height, values

of $-\Delta B_{rc}^2/\Delta B_{zc}^2$ were calculated. Weighted averages of the results at several heights are listed in Table 14 with errors in most cases determined from dispersion of the results. Within experimental errors, the anisotropy appears to be the same for all lattices. A reasonable average is 1.05 ± 0.03 .

Migration Area: Bettis Critical Experiments

The existence of anisotropy, if it is significant, must be taken into account in inferring the migration area. Within the one-group description, and with the anisotropy A defined above (M_z^2/M_r^2):

$$\rho = 1 - \frac{1 + M_r^2 B_r^2 + M_z^2 B_z^2}{k_\infty} = 1 - \frac{1 + M_r^2 (B_r^2 + A B_z^2)}{k_\infty} \quad (10)$$

If $B_g^2 = B_r^2 + A B_z^2$ is defined to be the buckling, then:

$$\left[\frac{\partial \rho}{\partial B_g^2} \right]_{\rho=0} = \frac{-M_r^2}{1 + M_r^2 B^2} \text{ where, at } \rho = 0$$

$$B_g^2 = B^2$$

$$k_\infty = 1 + M_r^2 B^2$$

$$\text{note: } \left[\frac{\partial \rho}{\partial B_r^2} \right]_{B_z^2} = \frac{\partial \rho}{\partial B_g^2}; \left[\frac{\partial \rho}{\partial B_z^2} \right]_{B_r^2} = A \frac{\partial \rho}{\partial B_g^2}$$

$$\text{Thus } M_r^2 = \frac{-\frac{\partial \rho}{\partial B_r^2}}{1 + B^2 \frac{\partial \rho}{\partial B_r^2}} = \frac{-\frac{1}{A} \frac{\partial \rho}{\partial B_z^2}}{1 + B^2 \frac{1}{A} \frac{\partial \rho}{\partial B_z^2}} \quad (11)$$

Table 15 lists the values of $\delta\rho/\delta B_r^2$ and $1/A \delta\rho/\delta B_z^2$ used in calculating the migration area. These numbers are averaged where both exist for a given lattice. The resulting M^2 is also listed in the table. Because of dispersions in the measured values of $\delta\rho/\delta B_r^2$, it is difficult to assign a realistic error to M^2 , and an estimated error of $\pm 4\%$ has been allowed for all. It is encouraging to note that $\delta\rho/\delta B_g^2$ as obtained from radial buckling changes and axial buckling changes appear to agree. This is particularly gratifying since the experimental technique of these two measurements were quite different.

Four-Factor Interpretation

The measured quantities have been presented in a form suitable for incorporation into any method of analysis, including the conventional four factor treatment. Four factor analysis has however limited usefulness and validity in dealing with the general class of problems which arise in the design of reactors of this kind. Therefore, although the analysis has been performed, it is not presented here. It may however be stated that a previous conclusion² still seems valid: a four factor interpretation is self-consistent if the values of η which are used are those based on a choice of 1.309 for natural uranium.

Table 14. Anisotropy of Migration Area

Lattice designation Fuel	W/U	$\langle A \rangle = M_z^2/M_r^2$ (Weighted average)
U metal 1.3%, 0.387 in.	2	1.07 ± 0.05
UO ₂ , 7.53 gm/cm ³ 1.3%, 0.601 in.	3	1.08 ± 0.05
UO ₂ , 7.53 gm/cm ³ 1.3%, 0.601 in.	4	1.04 ± 0.01
UO ₂ , 7.53 gm/cm ³ 1.3%, 0.601 in.	5	1.00 ± 0.03
UO ₂ , 7.52 gm/cm ³ 1.3%, 0.388 in.	4	1.04 ± 0.03
	5	1.06 ± 0.03
UO ₂ , 10.53 gm/cm ³ 1.3%, 0.383 in.	3	1.06 ± 0.03
UO ₂ , 10.53 gm/cm ³ 1.3%, 0.383 in.	3.6	1.04 ± 0.03
UO ₂ , 10.53 gm/cm ³ 1.3%, 0.383 in.	5	1.04 ± 0.01

Table 15. Migration Area, M^2 (Bettis)^a

Lattice designation Fuel	W/U	$\delta\rho/\delta B_r^2$ (cm ²)	$(1/A) \delta\rho/\delta B_z^2$ (cm ²)	M^2 (cm ²)
U metal 1.3%, 0.600 in.	2	-28.2	—	34.1
U metal 1.15%, 0.600 in.	2	-26.9	—	30.9
U metal 1.3%, 0.387 in.	2	-29.0	—	34.2
	3	-29.9	—	36.2
UO ₂ , 7.53 gm/cm ³ 1.3%, 0.601 in.	3	-46.1	-46.6	53.4
	4	-44.9	-45.7	52.5
	5	-41.1	—	46.7
UO ₂ , 7.52 gm/cm ³ 1.3%, 0.388 in.	4	-47.3	—	53.7
	5	-48.2	—	54.9
UO ₂ , 10.53 gm/cm ³ 1.3%, 0.383 in.	3	-39.1	-40.5	45.8
	3.6	-38.6	-37.9	44.3
	5	-35.4	-35.8	40.6

^a See text for estimated accuracy.

THEORETICAL SECTION

The purpose of this section is to describe the theory as it now stands and to compare its predictions with the experimental results. Two sources of error in theoretical results are obviously present, one from uncertainties in the microscopic cross-section information, the other inherent in the approximations chosen to simplify the transport equation. In hydrogenous systems, the former is known to be appreciable, since agreement is not secured between measured and rigorously calculated second moments of fission neutrons in pure water. The effect of approximations is difficult to appraise in that many specific and unrelated approximations must be introduced in any

calculation of core characteristics. The analysis presented here attempts a systematic, low-order approximation of all the apparent major effects encountered in slightly enriched uranium water lattices.

The greatest obstacle in the way of a highly simplified treatment of these systems is the relatively strong interaction between fission, capture, and leakage by fast neutrons. A large variety of models has been suggested to account for the experimental observations, many of which have the advantage of simplicity but few of which are generally applicable and all of which have contributed to confusion concerning the meaning of various synthetic parameters, such as resonance escape, migration area, etc. As an alternative to this approach, the present analysis provides a direct comparison of measured and computed quantities to avoid intruding involved questions of interpretation in the comparison. Because of the geometrical simplicity of the particular experiments considered here, a fairly precise approximation to the transport equation is practicable without extensive computational effort.

In reactor design, geometrical complexities impose a severe burden on present day computing equipment; under these conditions, a few-group treatment of the neutron energy spectrum has distinct advantages if it is capable of the precision required in design. To be of use, any model must be capable of extension to multi-region cores, a circumstance which eliminates many plausible schemes which are applicable to essentially bare cores. We shall not dwell on a detailed inter-comparison of such models, but present one which is consistent with the multigroup results and which has been extensively used in the evaluation and design of a number of hydrogenous reactors.

Description of the Theory

The theoretical treatment begins from a spherical P_1 approximation to the transport equation, which deals with homogenized neutron properties and contains self-shielding factors to allow for those features which homogenization would ordinarily suppress. The arguments for homogenization are these: Over most of the energy range of significance (0-10 Mev), the diffusion length in the core is large compared to the cell dimensions. At such energies, the flux cannot respond to the rapid variation of material properties; for practical purposes, the cell fine structure can be averaged out. At those energies where the diffusion length is small or comparable to the cell dimensions, it is possible to approximate the effect of the fine structure by means of a suitable shielding factor. For the fuel dimensions of interest here, only in the resonance region of U²³⁸ and at thermal energies is this necessary. The lattice as a result is approximated by a quasi-homogeneous medium, with uniform cross sections which may depend on the fine structure parameters.

Consider then the problem of determining the multiplication in a particular reactor, a one-dimen-

sional slab consisting of a central lattice region embedded in a reflector. The lattice consists of alternating slabs of moderator and fuel (Fig. 1). The homogenization is accomplished by integrating the transport equation over a lattice cell. If the

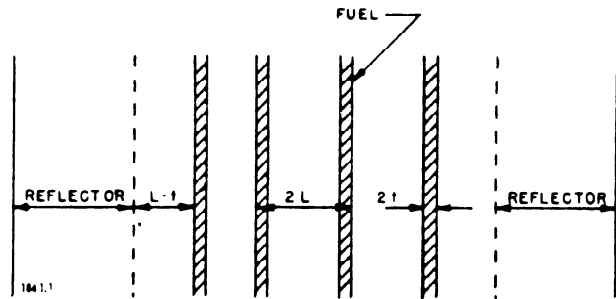


Figure 1. Slab lattice geometry

homogenized flux is defined as the average value over a cell,

$$\bar{\phi}(x, u, \mu) = \frac{1}{2L} \int_{x-L}^{x+L} dx' \phi(x', u, \mu) \quad (12)$$

and the average of any cross-section or other similar quantity is defined as the flux weighted mean value, the transport equation is transformed to a form in which the averaged values operate on the average flux.

The self-shielding factors which are introduced are defined by expressions of the form:

$$L_a(x, u, \mu) = \frac{1}{\Sigma_{ha}(u)} \frac{\int_{x-L}^{x+L} \Sigma_a(x', u) \phi(x', u, \mu) dx'}{\int_{x-L}^{x+L} \phi(x', u, \mu) dx'} \quad (13)$$

$$\Sigma_{ha}(u) = \frac{\Sigma_{1a}t_1 + \Sigma_{2a}t_2}{L} \quad (14)$$

The absorption cross-sections Σ_{1a} and Σ_{2a} are those of fuel and moderator, respectively. A shielding factor for scattering (L_s) may be obtained by replacing the absorption cross-sections in Eqs. (13) and (14) with scattering cross-sections.

It is assumed that over most of the spectrum ϕ does not vary sufficiently across a cell to make the shielding factors significantly different from unity. Near the resonances of U²³⁸ and at thermal energies, where shielding is important, the slow variation with position of $\bar{\phi}$, and the small diffusion length, permit the approximation of the shielding factors with those computed for an infinite lattice. Moreover, in practice the replacement of $L_a \Sigma_{ha}$, the angular weighted cross-section, by a scalar flux weighted cross-section, is also permissible. This is easily seen in a P_1 approximation; the scalar flux weighted absorption cross-section preserves the neutron balance and only introduces an error in the transport cross-section.

But neutrons of energies at which shielding is important cannot diffuse over large distances, and therefore cannot contribute greatly to leakage. These same remarks dispose of the necessity for flux weighting scattering cross-sections.

Using these approximations, we are led to consider a simpler transport problem in which the lattice is replaced, through a redefinition of the pertinent cross-sections,^{13, 14} by an effectively homogeneous core in a water reflector.

A further feature of the treatment is one which is common to all multigroup calculations. That is, the time-independent transport equation is replaced by an eigenvalue problem:

$$L\phi = \frac{1}{\lambda} S\phi \quad (15)$$

where the operator L provides the rate at which neutrons are removed from unit intervals of the variables x, u, μ by transport, absorption, and slowing-down, and S describes the rate at which fission replaces them. In the stationary state, these must be equal, and so the problem solved is the determination of the core size which leads to an eigenvalue of unity. Only when $\lambda = 1$ can $\phi(x, u, \mu)$ be identified with the flux in the reactor. The deviation of the largest eigenvalue from unity is readily seen to be the fractional amount by which the number of neutrons per fission must be reduced to make a stationary state possible in an otherwise specified core. In accord with common practice, λ will be referred to as the effective multiplication constant, although in general it does not rigorously correspond to any multiplication rate identifiable in the reactor.

Most of the measured properties of the critical core can be computed in the P_1 approximation under the following additional assumptions:

1. Thermal neutrons can be treated by one group diffusion theory.
2. It is possible to choose the top energy of the thermal group so that no scattering out of the group occurs, but assumption (1) remains valid.
3. The slowing down density at the top of the thermal group is isotropic in the laboratory reference frame.

These assumptions in addition to being traditional are plausible in view of the small diffusion lengths which occur at epithermal and thermal energies and the fact that the absorption cross-sections in this region have nearly the same energy dependence.

4. In the absence of sources and far from boundaries, the time independent flux is separable in space and energy.

This assumption is implicit in the comparison of results of exponential and critical experiments, which requires the central spectrum to be independent of detector and reflector properties. As a consequence of this assumption, the (scalar) flux and current are sinusoidally distributed in the slab geometry:

$$\begin{aligned} \phi(x, u) &= 2\pi \int_{-1}^1 d\mu \phi(x, \mu, u) = \cos Bx \phi(u) \\ J(x, u) &= 2\pi \int_{-1}^1 \mu d\mu \phi(x, \mu, u) = \sin Bx J(u) \end{aligned} \quad (16)$$

where B is a property of the material. This last assumption permits a calculation of the neutron spectrum near the center of the critical core which is independent of the reflector properties.

The basic equations of the treatment are then the P_1 set:

$$\begin{aligned} BJ(u) + \Sigma(u)\phi(u) - \int_0^u du' K_0(u' \rightarrow u)\phi(u') = \\ \frac{1}{\lambda} \sum_j \left[f(u)(1 - \beta^j) + \sum_i \delta(u - u_i) \beta_i^j \right] \\ \times \left[\int_0^{u_i} du' v_j(u') \Sigma_i^j(u') \phi(u') + \eta f \Sigma_s \phi_s \right] \end{aligned} \quad (17)$$

$$-B\phi(u) + 3\Sigma(u)J(u) - 3 \int_0^u du' K_1(u' \rightarrow u)J(u') = 0 \quad (18)$$

$$D_s B^2 \phi_s + \Sigma_s \phi_s = q(u_t) \quad (19)$$

The scattering kernels K_0 and K_1 are moments of the basic kernel K :

$$K_0(u' \rightarrow u) = 2\pi \int_{-1}^1 d\mu K(u' \rightarrow u, \mu), \quad (20)$$

$$K_1(u' \rightarrow u) = 2\pi \int_{-1}^1 \mu d\mu K(u' \rightarrow u, \mu), \quad (21)$$

and $q(u_t)$ is the slowing down density at the top of the thermal group (lethargy u_t),

$$q(u_t) = \int_{u_t}^{\infty} du \int_0^{u_t} du' K_0(u' \rightarrow u)\phi(u'), \quad (22)$$

D_s, Σ_s are the thermal diffusion coefficient and absorption cross-section, respectively;

f is the number of thermal neutrons captured in fuel per thermal neutron capture;

η is the number of fast neutrons emitted per thermal neutron captured in fuel.

$f(u)$ is the spectrum of prompt neutrons, assumed independent of both the isotope undergoing fission and the energy of the inducing neutron.

β^j is the fraction of neutrons delayed in emission from fission of the j th isotope.

B_i^j is the delay fraction in group i :

$$\sum_i \beta_i^j = \beta^j$$

Σ_i^j, v_j are the macroscopic fission cross-section, and number of neutrons per fission, respectively, for the j th isotope.

$\Sigma(u)$ is the total macroscopic neutron cross-section.

The Eqs. (17) through (19) describe a bare core with geometrical buckling B^2 . The spectrum and multiplication constant associated with a given buckling can be expressed in terms of the solution to a slowing down problem, with source strength normalized to unity over the fission neutron energy distribution.⁹ In terms of the normalized slowing down spectrum, denoted by subscript ∞ , the multiplication constant is:

$$\lambda(B^2) = \frac{fq_{\infty}(B^2)}{1+L^2B^2} + \sum_j \int_0^{u_j} du \nu^j(u) \Sigma_r^j(u) \phi_{\infty}(B^2). \quad (23)$$

The significance of the terms is clear. If a generation of neutrons is followed through the cycle birth to leakage or absorption, the first term represents the source from neutrons which succeed in reaching thermal energies, the second from those which are absorbed before entering the thermal spectrum. The second term must be retained in analyzing the neutron behavior of these systems, because they display such a large amount of epithermal fission.

The material buckling of the core can be obtained from a series of slowing down calculations; that B^2 which leads to a λ of unity is the material buckling, and the associated spectrum is that near the center of the core of both the exponential and critical experiments.

Few Group Theory

The application of the type of theory just described to multiregion or reflected cores can be made by straightforward multigroup methods. In hydrogen moderated cores, however, the strong coupling of various neutron energies produced by the large degradation occurring in hydrogen collisions permits the use of broad lethargy groups without significant losses in accuracy.

The essential point of the few group scheme described here is very simple. The spatial distribution of all fast neutrons in a given medium is taken to be sinusoidal and the energy spectrum is calculated in the P_1 approximation. The equations are then integrated over broad energy bands and, from the known spectra for this given spatial distribution, effective group constants are constructed. These broad groups can be defined in a variety of ways, but the only useful forms are those with group constants which are insensitive to the wave number of the spatial mode chosen. The few group eigenvalue problem for a multiregion system is then solved using constants defined in this way for the fast groups in each region.

From the solution of the set of Eqs. (17), (18) for a given spatial mode, a function $D(u)$ can be defined relating the current and flux gradient,

$$D(B, u) = J(B, u)/B\phi(u)$$

so that (17), (18) can be replaced by:

$$[D(u, B)B^2 + \Sigma(u)]\phi(u) =$$

$$\frac{f(u)}{\lambda} \left[\int_0^{u_t} du' \nu(u') \Sigma_r(u') \phi(u') + \eta f \Sigma_s \phi_s \right] + \int_0^u du' \Sigma_0(u', u) \phi(u') \quad (24)$$

Here the source term has been simplified by letting the delayed and prompt fission spectra be the same. Integration over lethargy bands $u_n < u \leq u_{n-1}$ results in the few group equations.

As mentioned before, the thermal group is chosen to be wide enough that neutrons in the "thermal" group are not scattered up into any of the "fast" groups. If the reactor is also large enough for the P_1 approximation of the slowing down process to be applicable, two, three, or four broad groups of neutrons appear to provide a description of the variation of neutron spectrum in space which is adequate for most design purposes. If in fact the lethargy widths of the intermediate groups are chosen large enough such that $\exp[u_{n-1} - u_n] \leq 1$, cross coupling of the groups can be neglected even for hydrogen scattering and the directly coupled equations for an n -group scheme results:

$$[D_n B^2 + \Sigma_{an} + \Sigma_{rn}] \phi_n = X_n \sum_m [\nu \Sigma_{tm} \phi_m + \Sigma_{r(n-1)} \phi_{(n-1)}] \quad (25)$$

$$[D_s B^2 + \Sigma_{as}] \phi_s = \Sigma_{r(m-1)} \phi_{(m-1)}$$

Here, the removal cross-section is defined as

$$\Sigma_{rn}(B) = \int_{u_n}^{u_{n+1}} du' \int_{u_{n-1}}^{u_n} du' \Sigma_{s0}(u', u) \phi(u', B) / \phi_n(B), \quad (26)$$

and

$$\phi_n(B) = \int_{u_{n-1}}^{u_n} du' \phi(u', B)$$

$$D_n(B) = J_n / B \phi_n \quad (27)$$

$$\Sigma_{an}(B) = \int_{u_{n-1}}^{u_n} du' \Sigma_a(u') \phi(u', B) / \phi_n$$

$$\Sigma_{tn}(B) = \int_{u_{n-1}}^{u_n} du' \Sigma_t(u') \phi(u', B) / \phi_n$$

$$X_n = \int_{u_{n-1}}^{u_n} du' f(u')$$

No general group width criterion can be given for inelastic scattering, but if the condition for hydrogen is met, the range of inelastic degradation will usually be small in lethargy (usually $\Delta u < 5$ for a lethargy scale $u = \ln(10 \text{ Mev}/E)$) compared to the combined width of the first two high energy neutron groups.

Now it is obvious that if the solution of the eigenvalue problem for a bare core with buckling B^2 is desired, either a multigroup form of the P_1 Eqs. (17-19) or the few group Eq. (25) could be employed and, if the group constants were calculated for the correct mode, would yield identical results. Further, if the

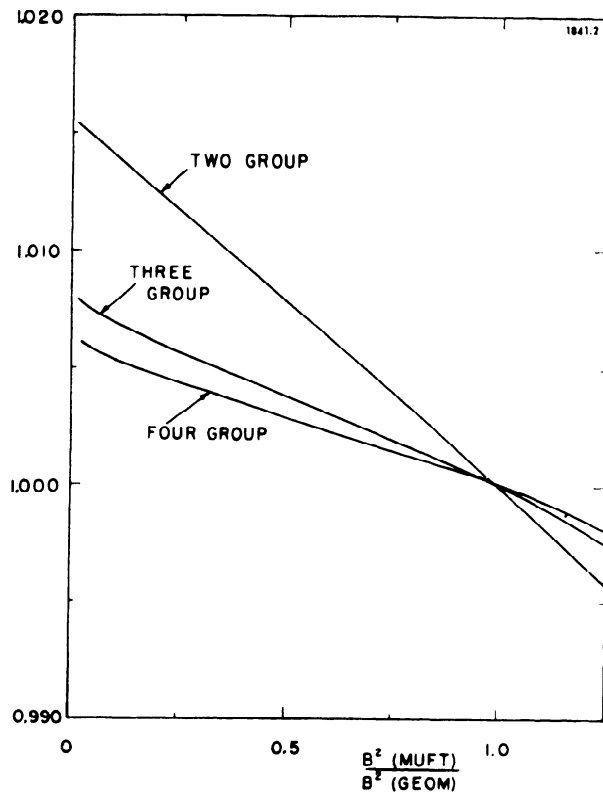


Figure 2. Few group eigenvalues of a bare core

group constants were entirely independent of B , the inverse problem of determining the critical size of a bare reactor could be solved without iteration using the group constants computed for any buckling.

In practice, the group constants are not entirely independent of B , so that various group schemes will give differing eigenvalues. In Fig. 2, an example is given of a typical slightly enriched bare core, the eigenvalue being given for two, three, and four group models as a function of the buckling used in computing the group constants by the MUFT-III code described later. It will be noticed that the four group eigenvalue exhibits about half the error shown by the two group model; this type of behavior is generally observed with P_1 group constants. The spread between two and four group eigenvalues is most pronounced for small reactors and, of course, decreases as the reactor increases in size since the leakage becomes less important. Because of the way the group Eqs. (25) are obtained, the differences between eigenvalues vanish for a critical system.

In the computation of the eigenvalue of a multi-region reactor, the P_1 few group result is no longer identical with that given by the P_1 multigroup calculation and very little can be said about the precision of the few group scheme in general. It is observed in typical cases, such as the water reflected slab core shown in Fig. 1, that the same trends in eigenvalue accompany changes in the buckling used in computing the core group constants as are found for a bare core. But there is also a small dependence of the

eigenvalue on the buckling chosen in the computation of the reflector group constants. If the latter has an important effect in a particular case, the application of the few group scheme becomes questionable, for the equations used in computing the group constants do not apply in the reflector.

Special Forms of the Group Equations

Several useful reductions of the eigenvalue Eq. (25) are often used which involve physically descriptive parameters such as the resonance escape, fast fission factor and age. Although the definition of these parameters is not unique, they can be precisely stated for any given model in terms of reaction rates and slowing down density. The range of applicability of the model then depends on how invariant the presumed "constants" are to the buckling of the system. Several such reductions are described here.

Special Cases

We consider the situation implied by taking only one fast group. Designating this by subscript 1, and the thermal neutron group by 2, one finds that (25) can be rewritten for a bare reactor as:

$$\lambda = \frac{(\eta f)_1(1 - \rho_1)}{(1 + \tau B^2)} + \frac{(\eta f)_2 f_1}{(1 + L^2 B^2)(1 + \tau B^2)} \quad (28)$$

with the definitions from (27):

$$\begin{aligned} (\eta f)_1 &= \frac{\nu \Sigma_{f1}}{\Sigma_{a1}} & (\eta f)_2 &= \frac{\nu \Sigma_{f2}}{\Sigma_{a2}} \\ \tau &= \frac{D_1}{\Sigma_{r1} + \Sigma_{a1}} & L_2 &= \frac{D_2}{\Sigma_{a2}} \\ \rho_1 &= \frac{\Sigma_{r1}}{\Sigma_{r1} + \Sigma_{a1}} \end{aligned}$$

This arrangement describes conveniently both thermal and intermediate reactor systems without treating the fast effects as small corrections applied to the thermal neutron terms. It will be noticed that fast fissioning does not augment the neutron age: no internal fast cycling occurs because the fissions in both groups are treated in a similar way.

The four factor two group model is a further reduction of (25) which has been widely used in both reactor design and the analysis of critical experiments. In applying this model to U^{235} — U^{238} mixtures no explicit mention of the fast fission in U^{235} is made, so that, as will be seen, a peculiar definition of the resonance escape probability P_R is required. The fast fission and capture in U^{238} above the fission threshold at 0.8 Mev is represented by a factor ϵ , the latter being defined as the number of neutrons slowing down past the U^{238} fission threshold per neutron produced in other than U^{238} fission.

This method of treating the fast effect in U^{238} was convenient in early calculations of graphite systems in which little coupling between adjacent fuel elements occurred. The fast multiplication was treated as a

separate internal chain reaction dependent primarily on the geometry of the single element, the problem then being solved by a monoenergetic successive generation treatment. However, in water moderated systems, the close packing which results in large buckling also produces strong fast neutron coupling between fuel elements.

To reduce the two group form of (25) to the four factor model, let the fast group be split into one band above (superscript 1) and one below (superscript 2) the U²³⁸ threshold. Further, let the absorption in the lower band be separated into a part proportional to the U²³⁵ fission and a residual part, Σ_{a1}^{2R} .

$$\begin{aligned}\Sigma_{a1}^1 \phi_1 &= \int_0^{u_1} dt \Sigma_a(u) \phi(u, B), \\ \Sigma_{a1}^2 \phi_1 &= \int_0^{u_2} dt \Sigma_a(u) \phi(u, B), \text{ etc.} \\ \Sigma_{a1}^{2R} &= \Sigma_{a1}^2 - \frac{\nu \Sigma_{f1}^2}{(\eta f)}\end{aligned}$$

Here (ηf) is the neutron production per neutron absorbed in the thermal group.

The source term in the fast group equation can be written as:

$$\frac{\eta f \epsilon}{\lambda} \frac{\Sigma_{r1} + (\nu \Sigma_{f1}^2 / (\eta f))}{\Sigma_{r1}} \Sigma_{a2} \phi_2$$

preserving the definition of the fast fission factor described above.

$$\epsilon = 1 + \frac{(\nu \Sigma_{f1}^1 - \lambda \Sigma_{a1}^1) \phi_1}{\nu \Sigma_{f2} \phi_2 + \nu \Sigma_{f1}^2 \phi_1} \quad (29)$$

Since the coefficient of Σ_{a1}^1 is taken to be $\lambda = 1$, the variation of ϵ with buckling (or reactor period in the time dependent case) within the four factor model will be different from that given by (25), even in a bare reactor, as in (28).

The familiar four factor equations are now obtained by letting:

$$\Sigma_1 = \Sigma_{r1} + \Sigma_{a1}^{2R} + \nu \Sigma_{f1}^2 / \eta f$$

and defining

$$P_t = \Sigma_{r1} / \left(\Sigma_{r1} + \frac{\nu \Sigma_{f1}^2}{\eta f} \right)$$

We then have:

$$[D_1 B^2 + \Sigma_1] \phi_1 = \frac{\eta f \epsilon}{\lambda P_t} \Sigma_{a2} \phi_2, \quad (30)$$

$$[D_2 B^2 + \Sigma_{a2}] \phi_2 = P_R P_t \Sigma_1 \phi_1,$$

with the resonance escape P_R being given as the probability of escaping capture by the cross sections which contribute to Σ_{a1}^{2R} :

$$P_R = \Sigma_1 - \Sigma_{a1}^{2R} / \Sigma_1, \quad \tau = D_1 / \Sigma_1 \quad (31)$$

The critical equation for the four factor form of the two group equations is then independent of P_t and explicit mention of epithermal U²³⁵ fission disappears:

$$\lambda = \frac{\eta f \epsilon P_R}{(1 + \tau B^2)(1 + L^2 B^2)} \quad (32)$$

From comparing the two critical Eqs. (28) and (32), it is clear that the ages and migration areas $(\tau + L^2)$ appearing in the two expressions differ in a way dependent on the amount of absorption occurring at energies above the U²³⁸ fission threshold. If the implicit dependence of λ on is retained in (32), this critical equation is identical with (28). More important, however, is the difference between the "resonance escape" probabilities, for in (28) p_1 represents the probability of escaping fast absorption by any process (fission or capture) whereas in (32) P_R accounts only for these absorptive events which are neither included in ϵ nor proportional to the $\nu \Sigma_{f1}^2$ of U²³⁵. In multiregion systems the factor P_t cannot be ignored in Eq. (30) since it effects, in a sense, a flux renormalization.

Although the definition of P_R appears at first sight to be rather involved, it is particularly convenient for U²³⁵—U²³⁸ systems of low enrichment. As the example below shows, P_R corresponds rather closely to the resonance escape probability of a system containing U²³⁸ as the only absorber but with the $1/v$ continuation of the thermal U²³⁸ capture cross section subtracted. Actually it includes as well about half of the epithermal U²³⁵ capture effects.

The following illustrative case is taken from a MUFT-III calculation of the fast constants of a TRX 1.0% enriched lattice of 0.600 in. diameter rods with a water to uranium volume ratio of unity. The resonance self-shielding factor was $L = 0.635$ and the buckling $B^2 = 9.66 \times 10^{-4} \text{ cm}^{-2}$. For Eq. (28), the constants of importance are:

$$\tau = 31.2 \text{ cm}^2 \quad p_1 = 0.529,$$

and the fast and thermal contributions of λ are

$$\lambda = 0.303 + 0.716 = 1.019.$$

For Eq. (32), the appropriate constants obtained using the definitions (29) and (31) are:

$$\epsilon = 1.110 \quad P_R = 0.680 \quad \tau = 33.6 \text{ cm}^2$$

which result in $\lambda = 1.018$. Now if the usual simple calculation of the resonance escape probability is made, considering only the U²³⁸ and water in the mixture and using the MUFT-III cross-sections, one gets:

$$p = \exp[-L(RI)] = 0.648$$

In terms of effective resonance absorption cross-section, this difference in p amounts to about 1.3b. The effective resonance absorption cross-section of the $(1/v)$ continuation of the thermal U²³⁸ cross-section is about 1.1b.

Description of Computational Techniques

MUFT-III

This code evaluates the group constants of a

fifty-four group calculation, and then uses the quantities so generated to solve the slowing-down Eq. (23). The group constants are found by integrating and averaging the appropriate terms in Eqs. (17) and (18). The input data are a trial buckling, the atom concentrations of the uranium, hydrogen, etc., and a self-shielding factor. The output data are the group constants, the eigenvalue, the flux distributions, and (as desired) few group parameters. The code is written for the IBM-650. For numerical solution, the Eqs. (17), (18) are converted to multigroup equations by integration over narrow lethargy bands. Since fission cycling has no effect on the fast neutron spectrum, the source term can be replaced simply by the prompt fission spectrum $f(u)$ for criticality calculations or by the delayed neutron spectrum $\delta(u-u_i)$ for effective β_i' calculations.

The scattering integrals are broken up into three terms associated with hydrogen recoil scattering, "heavy" element recoil scattering and inelastic scattering. Since the latter has in general no simple analytical form, it is represented by a matrix of group transfer coefficients for each element. Only the second term introduces further approximation through the use of an age theory expansion, but its effect in water moderated systems is usually small. The hydrogen scattering integrals require no further approximation.

In the MUFT codes, the approximate homogeneous absorption integral is evaluated by integrating the analytic hydrogen moderated flux shape within the group over a Breit-Wigner single resonance shape, neglecting the effect of leakage within the group on the absorption rate. This absorption rate is then made proportional to the slowing down density at the top of the group. To convert this homogeneous estimate into an accurate resonance absorption term, an L factor is available as input which introduces the changes in resonance integral produced by lumping and Doppler effects.

SOFOCATE Code

This is a multigroup code written for the IBM-704 which calculates the energy distribution of neutrons in the homogenized core in the neighborhood of thermal energy. The characteristics of the moderator are idealized by representing energy interchange by the symmetrical component of the scattering kernel of hydrogen gas with a Maxwellian velocity distribution. For an infinite medium, the treatment thus follows the Wigner-Wilkins solution with the slight modification that the absorption cross sections need not be $(1/v)$. In a finite medium, leakage is included using the assumption that no anisotropic energy interchange occurs on scattering. The diffusion constant is calculated as a function of energy by a scheme proposed by A. Radkowsky; the observed variation with energy of the scattering cross-section of bound hydrogen is used to obtain an effective mass from which in turn an average cosine of the scattering angle results and thus a diffusion constant is found.

The justification of the use of this highly idealized model of the low energy spectrum rests on the comparison of calculated and observed energy distributions and thermal diffusion lengths. Amster¹⁰ has compared Wigner-Wilkins calculations of the neutron spectrum in solutions of boric acid and water with Poole's¹¹ time of flight measurements and has found good general agreement in the shape of the distributions. No systematic discrepancies were apparent even up to concentrations of 10 barns/hydrogen atom. The model described above was also found by Amster to yield values of the thermal diffusion length in pure water, and its temperature variation, which are in substantial agreement with experimental results.

The effect of core fine structure on the thermal spectrum calculation is difficult to assess; the homogeneous spectrum is somewhat too hard for the moderator—too soft for the fuel. The calculation should, in any case, represent a better compromise than a Maxwellian at reactor temperature.

Calculations of Self-shielding Factors

To avoid the introduction of a large error not inherent in the reactor model, the criticality calculations employed a smoothed set of experimental thermal disadvantage factors based on data from Bettis and BNL.

Resonance self-shielding factors were computed with the aid of a UNIVAC Monte Carlo code. The code treats a cylindrical rod in a hexagonal cell; the rod is surrounded by a void which approximates the air gap and aluminum cladding. The resonances are Doppler broadened Breit-Wigner shapes with the $1/v$ tails suppressed, and all non-resonance capture is neglected since competition with a single resonance is small. The interference of potential and resonance scattering is also neglected, but slowing down by all elements is treated rigorously. The resonance parameters used in the calculation are essentially those in BNL-325, which cites 18 resolved resonances at energies up to 418 eV.

COMPARISON OF THEORETICAL RESULTS WITH MEASUREMENTS

In view of the large accumulation of data on the slightly-enriched metal and oxide rod lattices, it is not feasible to present curves showing the comparison of all theoretical and experimental results. Some comparisons for intensive parameters are shown in Figs. 3, 4 and 5. The theoretical values of the various lattice characteristics are given in Table 16 for comparison with experimental summaries appearing elsewhere in this paper. In general, the cell parameters are in fairly good agreement, but the attempts to measure the leakage effects seem subject still to large uncertainties. The predicted bucklings are all systematically high and the eigenvalues calculated for the experimental buckling show an enrichment dependence. Thus, although the theory appears to provide a low order approximation to these systems,

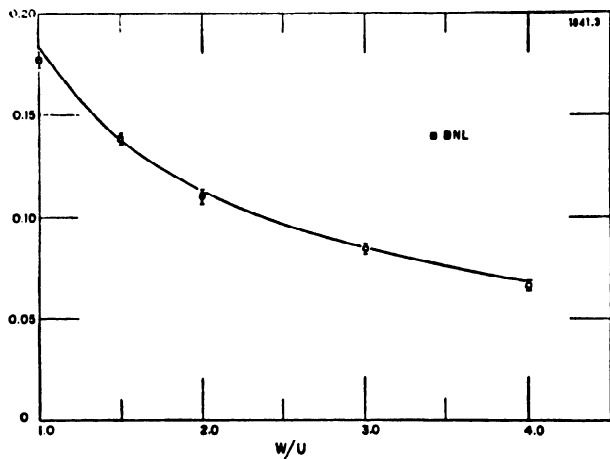


Figure 3. δ_{28} for 1.0%, 0.387 inch diameter lattices

the degree of precision attained in the complete description is not yet satisfactory.

Discussion of Cell Parameters

In order to avoid compounding confusion, the comparison presented here is made, as far as possible, in terms of the measured reaction rates. Thus Table 16 shows the primary data from which the synthetic parameters, ϕ , ϵ , etc., can be constructed with some additional information.

The theoretical prediction of these quantities is, of course, strongly dependent on the fission and capture cross-sections employed in the calculations. Although the thermal neutron cross-sections of U²³⁵ and U²³⁸ are rather well known, there are large gaps in the information available in the epithermal and fast neutron energy ranges. The cross sections chosen in general are consistent with data presented in BNL-325. The more important additions to this information

are the inelastic emission spectra for U²³⁸, which have been calculated roughly from the evaporation model, and the capture cross section between 450 ev and 30 kev, again in U²³⁸. The latter is an estimate of the average over resonances obtained from a continuation of the resonance structure observed below 450 ev. In U²³⁵, an average over resonances has been used throughout the entire energy range above thermal, since the concentrations are too low to exhibit marked self-shielding effects. The U²³⁵ resonance fission integral was normalized to the Hanford value¹² and the capture cross-section adjusted such that the ratio of capture integral to fission integral was roughly 0.4. The uncertainties of these fast cross-sections certainly lead to errors in the calculations comparable to the uncertainties in the theory.

The calculation of ρ_{28} , as is clear from earlier discussions, incorporates a combination of a Monte Carlo treatment of the resolved resonances below 450 ev and an average cross-section above this energy. This latter contribution should in principle be somewhat dependent on rod size and W/U ratio; however, the range of these variables covered in the present experiments is apparently not sufficient to produce a discernible dependence of this type. The rather gratifying agreement observed between the measurements and theory is primarily a consequence of the Monte Carlo results.

A large contribution to δ_{25} arises from fissions occurring in the neighborhood of the cadmium cut-off; thus δ_{25} is dependent on a detailed knowledge of the transmission curve and the U²³⁵ cross-section in this neighborhood. The problem of obtaining a precise correlation between what has been measured and calculated is, therefore, considerably more difficult than in the case of ρ_{28} .

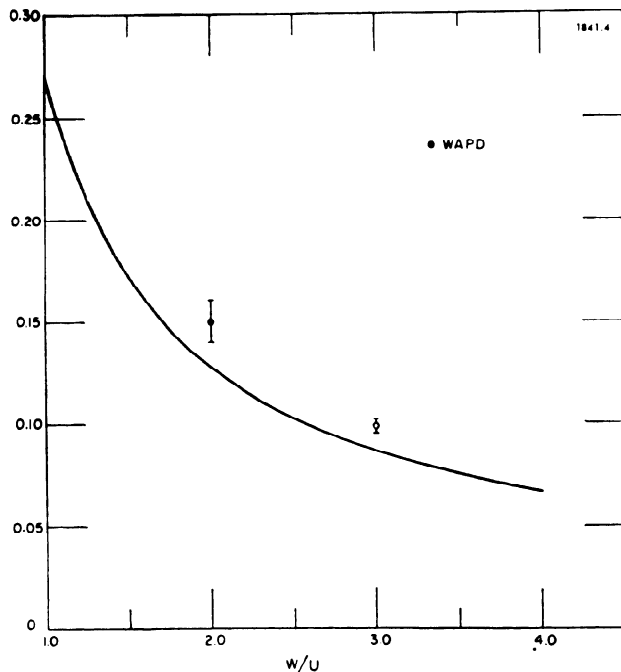


Figure 4. δ_{25} for 1.3%, 0.387 inch diameter lattices

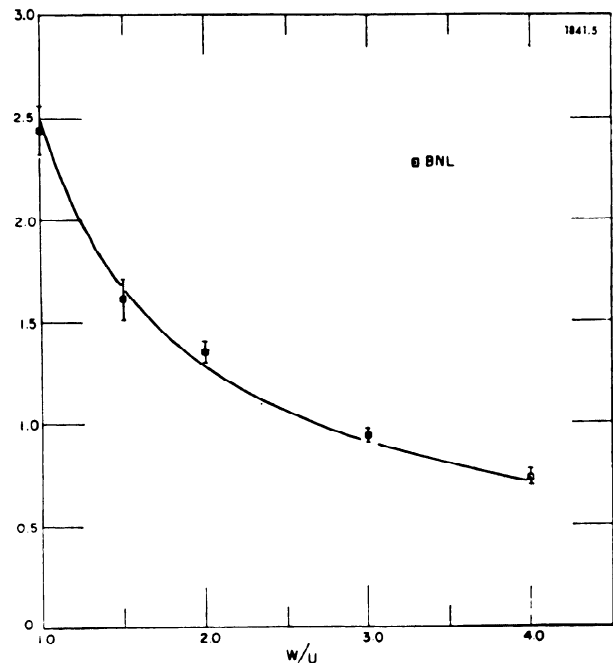


Figure 5. ρ_{28} for 1.0%, 0.387 inch diameter lattices

Table 16. Calculated Lattice Parameters^a

Rods		ρ_{28}	δ_{25}	δ_{28}	P_{38}	CR	η	f	M^* (cm^3)	B^* ($\text{cm}^{-1} \times 10^4$)	Reflector savings (cm)	λ (eigenvalue)	
0.600 in.	1.3%	2.88	0.259	0.172	0.610	0.932	1.5840	0.943	34.19	33.40	7.45	1.0038	
		1.87	0.171	0.132	0.714	0.744	1.5881	0.918	32.44	56.31	6.91	1.0120	
		1.41	0.128	0.107	0.774	0.649	1.5905	0.892	31.59	65.30	6.65	1.0109	
		1.00	0.088	0.080	0.836	0.559	1.5930	0.841	30.80	63.32	6.39	1.0057	
	1.15%	0.795	0.069	0.065	0.873	0.510	1.5936	0.791	30.49	51.67	6.26	1.0037	
		2.59	0.236	0.176	0.614	0.992	1.5380	0.939	34.04	24.31	7.37	1.0098	
		1.69	0.156	0.135	0.716	0.798	1.5412	0.913	32.30	45.57	6.87	1.0148	
		1.28	0.117	0.110	0.775	0.700	1.5443	0.885	31.44	53.37	6.61	1.0136	
	1.0%	0.915	0.081	0.082	0.838	0.607	1.5460	0.833	30.67	49.83	6.39	1.0069	
		0.727	0.063	0.067	0.874	0.557	1.5477	0.781	30.38	37.55	6.26	1.0041	
		2.35	0.219	0.180	0.618	1.05	1.4933	0.936	33.86	15.53		1.0188	
		1.55	0.143	0.137	0.719	0.853	1.4970	0.907	32.17	35.23	6.81	1.0161	
	0.357 in.	1.3%	1.18	0.109	0.113	0.777	0.752	1.4987	0.879	31.29	41.83	6.57	1.0163
			0.842	0.075	0.085	0.839	0.656	1.5017	0.825	30.52	37.29	6.37	1.0117
			0.670	0.059	0.070	0.875	0.604	1.5027	0.772	30.25	23.94	6.26	1.0082
			3.03	0.268	0.176	0.596	0.964	1.5844	0.947	37.23	26.71	7.87	1.0198
1.15%		2.00	0.172	0.133	0.697	0.780	1.5878	0.924	34.59	47.91	7.28	1.0232	
		1.54	0.128	0.108	0.755	0.685	1.5904	0.903	33.38	57.74	6.99	1.0145	
		1.07	0.087	0.080	0.824	0.579	1.5922	0.860	32.14	62.56	6.65	1.0086	
		0.838	0.067	0.064	0.863	0.523	1.5933	0.817	31.55	56.55	6.47	1.0048	
1.0%	2.73	0.241	0.178	0.600	1.03	1.5379	0.943	37.19	18.30	7.74	1.0147		
	1.82	0.156	0.135	0.700	0.837	1.5422	0.918	34.51	37.84	7.23	1.0199		
	1.40	0.116	0.110	0.757	0.738	1.5438	0.896	33.27	46.54	6.95	1.0124		
	0.977	0.079	0.082	0.826	0.627	1.5469	0.851	32.01	50.13	6.62	1.0107		
1.0%	0.768	0.061	0.066	0.864	0.571	1.5476	0.807	31.44	42.70	6.46	1.0059		
	2.48	0.223	0.183	0.604	1.09	1.4932	0.939	36.97	10.22		1.0251		
	1.66	0.144	0.139	0.703	0.892	1.4969	0.914	34.31	28.30	7.14	1.0280		
	1.28	0.108	0.113	0.759	0.790	1.4989	0.890	33.07	35.93	6.89	1.0210		
		0.898	0.074	0.085	0.827	0.678	1.5010	0.843	31.84	37.57	6.60	1.0177	
		0.708	0.057	0.068	0.865	0.619	1.5018	0.798	31.30	29.45	6.45	1.0106	

^a In each group, the values of W/U are listed in the order, 1, 1.5, 2, 3, 4.

The main advantage of the traditional separation of thermal effects into the factors η and f lies in the presumed independence of η with respect to all lattice parameters other than enrichment. The thermal utilization then includes all of the dependence on W/U and geometry. In reality, such a separation is not rigorously found, but in lattices such as those being considered, it still represents a rather good approximation. Recent measurements by Poole¹¹ have shown substantial difference in the effective neutron temperatures at the center of the rod and in the moderator; although this effect may not strongly effect η , it does raise serious questions concerning the validity of one group calculations of the flux shape in the cell.

Lacking an adequate solution to this problem, some insight into the magnitude of the effect can be had by examination of the dependence of η on the neutron spectrum in the homogeneous case.

The Wigner-Wilkins hardening of the thermal spectrum leads to a small but definite variation of η with water-to-metal ratio. Table 17 gives values for the 0.600 in. metal rods, and for a Maxwellian spectrum.

The hardening depresses the apparent value of η_{nat} from 1.328 in a Maxwellian spectrum, with the cross-sections used in the calculations, to 1.310 in the spectrum of the least watery cores. Since the hardening in the rods may be even more severe than is calculated for the homogeneous mixtures, the inference

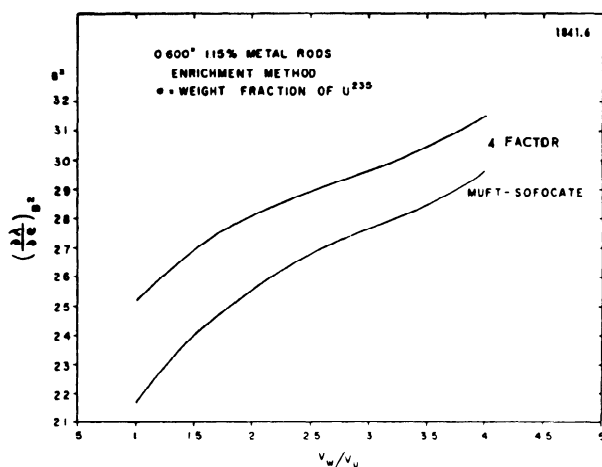
of a value of η_{nat} of 1.309 can presumably be explained on the basis of the spectrum changes.

Macroscopic Core Characteristics

The ability to predict the critical configuration of a core depends on the combination of effects typical of a cell, such as the reaction rates already discussed, with leakage from the system through the critical equation. This synthesis is complicated by the fact that some interaction between the cell effects and leakage occurs, thus making an analysis based on a strict separation impossible. Some experiments aimed at exploiting the near-separability are described elsewhere in this paper; the analysis and its attendant difficulties is discussed below. The degree of success achieved in the synthesis can be exhibited in a variety

Table 17. Effect of Flux Hardening on η

	1.3%	1.15%	1.0%
$W/U = 1.0$	1.5840	1.5380	1.4933
1.5	1.5881	1.5412	1.4970
2.0	1.5905	1.5443	1.4987
3.0	1.5930	1.5460	1.5017
4.0	1.5936	1.5477	1.5027
Maxwellian	1.598	1.552	1.507


 Figure 6. Four factor and multigroup calculations of $[\partial\lambda/\partial\epsilon]_B^2$

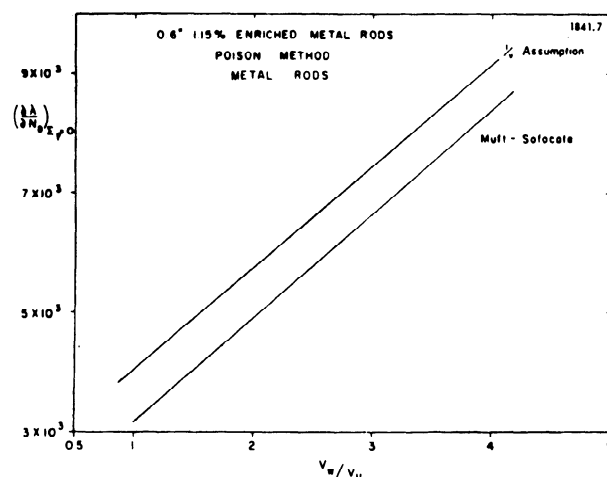
of ways, perhaps the most convenient of which is the predicted eigenvalue corresponding to the experimental buckling. In addition, because of its practical importance, the theoretical predictions of material buckling as a function of enrichment, rod size and water-to-uranium ratio are given to show the size of errors still inherent in the theoretical treatment.

Measurements of Migration Area

In the present discussion, an evaluation of the migration area measurements is made in terms of both the multigroup and few-group theories and the results compared with P_1 calculations of the leakage effects. In each of these experiments, a change in buckling, and therefore, leakage, is offset by some other alteration of the system; in the poison and enrichment measurements, the major compensating change occurs in the thermal cross-sections with lesser changes in the fast neutron cross-sections; in the differential water height measurement the buckling perturbation results in a rising flux in time which can be formally related to a change in the effective delayed neutron fraction.

The term "migration area" is used in the literature to cover a multitude of parameters, all having in common a close relation to the non-leakage probability but differing in detail. This is of the same nature as the confusion in connection with ϵ and β but is of somewhat more consequence in this case. There is a quantity which can be rigorously defined and which any successful few-group scheme should be capable of predicting which relates the change in λ to the change in buckling at the critical condition of the lattice. Because of the general significance of what we will call the "reduced migration area", we have chosen to analyze the experiments in terms of it rather than in terms of the directly measured quantities. Although this procedure combines uncertainties in the experiments with those arising from the theory, the latter are not strongly dependent on the description of leakage.

The reduced migration area,


 Figure 7. "1/v" and multigroup calculations of $[\partial\lambda/\partial N_B]_B^2$

$$\Lambda = - \frac{\partial\lambda}{\partial B^2}$$

where the partial derivative implies that composition is held fixed, is approximately related to the migration area in the two-group model by the formula

$$M^2 = \frac{1 + M^2 B^2}{\lambda} \Lambda + I_2^2 \frac{(\eta f)_1 (1 - \beta_1)}{(\eta f)_2 \beta_1}$$

It is worth noting that when ϵ is used in the four-factor formula without its implicit dependence on λ , it has a different physical significance and definition from that used in the multigroup critical Eq. (24) and the two-group Eq. (28). Although the measurements do not clearly indicate the importance of this effect, the example given earlier indicates that there is of the order of a 10% difference in associated values of M^2 .

The material buckling is observed at the enrichments ϵ_1 , ϵ_2 . Since in both cases B^2 corresponds to the stationary spatial distribution, there is no change in λ , and, if the changes are small,

$$d\lambda = 0 = \left[\frac{\partial\lambda}{\partial B^2} \right]_e dB^2 + \left[\frac{\partial\lambda}{\partial \epsilon} \right]_{B^2} d\epsilon,$$

so that

$$\Lambda = - \left[\frac{\partial\lambda}{\partial B^2} \right]_e = \left[\frac{\partial\lambda}{\partial \epsilon} \right]_{B^2} \left(\frac{\partial \epsilon}{\partial B^2} \right)$$

The enrichments and the bucklings are the direct experimental data. In addition to the inherent errors in these quantities, theoretical uncertainties enter through the evaluation of $(\partial\lambda/\partial\epsilon)_{B^2}$; the nature of these is apparent from Eq. (24).

$$\left[\frac{\partial\lambda}{\partial \epsilon} \right]_{B^2} = \frac{q}{1 + I_2^2 B^2} \frac{\partial \eta f}{\partial \epsilon} + \frac{\eta f}{(1 + I_2^2 B^2)} \frac{\partial q}{\partial \epsilon} + \frac{\partial I}{\partial \epsilon},$$

I being the epithermal fission neutron source integral. Most of the enrichment dependence is in the first term, but the changes in the fast group are important

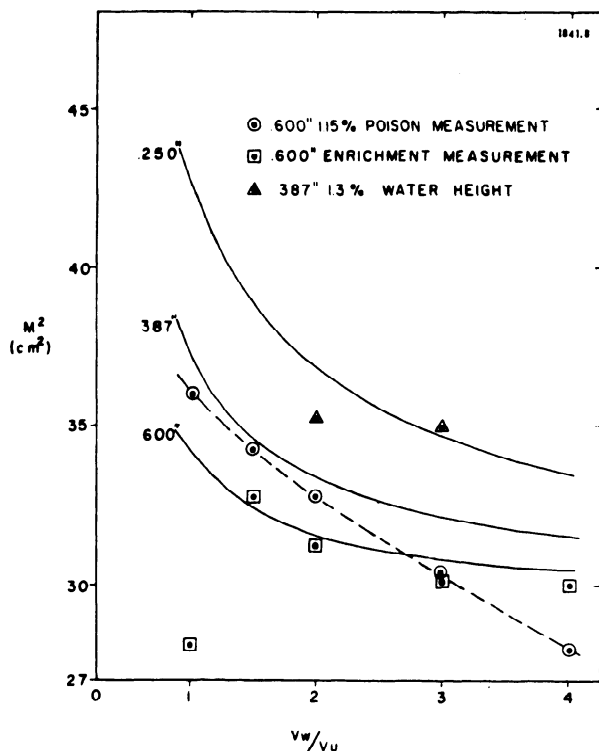


Figure 8. Multigroup and experimental values of M^2

also. The slow and fast contributions in one case, the 0.600 in., 1.15% metal rods at $W/U = 1$, are 17.7 and 4.0 cm^2 respectively. This can be contrasted with the purely thermal effect which leads to $(\partial\lambda/\partial\epsilon)_{B^2} = (1/\eta f) (\partial\eta f/\partial\epsilon) = 25 \text{ cm}^2$. This result is what would be obtained from the four factor formula if the η^{25} were constant with energy. Since this is not the case, some U^{235} epithermal captures are forced into P_R , causing a negative correction term. There is an additional effect arising from the dependence of ϵ in Eq. (29) on the flux spectrum, since the partial derivative is evaluated at constant buckling. The neglect of these lead to substantially higher migration areas inferred from the straightforward four-factor application than are obtained from the multigroup calculation of $(\partial\lambda/\partial\epsilon)_{B^2}$. The difference between these evaluations of $(\partial\lambda/\partial\epsilon)_{B^2}$ is shown in Fig. 6.

The analysis of the poison experiment proceeds along similar lines. Here, again, the effect of a detailed treatment of fast and epithermal fission is to decrease the sensitivity of the eigenvalue to the addition of boron, from that which results from the purely thermal evaluation. Because δ_{25} is very near that which would be given by a $1/v$ cross-section, the inclusion of boron in the system has little effect on the P_R which appears in the four-factor scheme. This still leaves a positive contribution to $(\partial\lambda/\partial N_B)_{B^2}$ from the change in ϵ which arises in the same fashion as in the enrichment experiment but is of the opposite sign. Calculations of $(\partial\lambda/\partial N_B)_{B^2}$ are shown in Fig. 7 as obtained from MUFT-SOFOCATE and also from the "1/v" assumption. Here N_B is the homogenized boron concentration in the core.

In a third class of experiment, the reactor dimensions are subjected to a small change, which makes the system supercritical. The reciprocal period ω is the measured quantity in this case. The relation of the measurement to $(\partial\lambda/\partial B^2)_{\omega=0}$ is a problem similar to that encountered in the poison experiment. After the decay of transients introduced by the perturbation, the flux distribution is again independent of time, and obeys a steady state transport equation differing from a true steady state by small changes in yield and fission spectrum.

The effective delayed neutron yields are given by:

$$\bar{\beta}_i = \frac{\beta_i^{25} + \delta_{28}\beta_i^{28}}{1 + \delta_{28}} \cdot \frac{\lambda_i}{\lambda} = \beta_i \frac{\lambda_i}{\lambda}$$

where δ_{28} is computed with the unperturbed spectrum, β_i^{25} and β_i^{28} are the delayed neutron yields of the respective isotopes, and λ_i would be the multiplication constant if all the neutrons were born with the energy of the delay group. The lower energy of the delayed neutrons makes itself felt chiefly through the reduced leakage probability and the loss of the fast effect. These effects oppose one another with the result that the effective yields differ from the true yields by about 5% or less. Calculated values of $\bar{\beta}_i/B_i$ for two of the 0.387 in. 1.3% enriched metal lattices are given in Table 18.

The values of $(\delta\lambda/\delta B^2)$ found from the various metal lattice experiments, using the MUFT-SOFOCATE calculations of the determination of the other partial derivative, are listed in Table 19. The migration areas inferred from these are compared with the calculated values in Fig. 8.

Material Buckling Calculations

A primary practical test of the theoretical model is the comparison of calculated and measured values of material buckling for the various lattices. The disagreement is of the order of 10% with the calculated bucklings always lying higher than those observed. Because of the tendency of the theory to

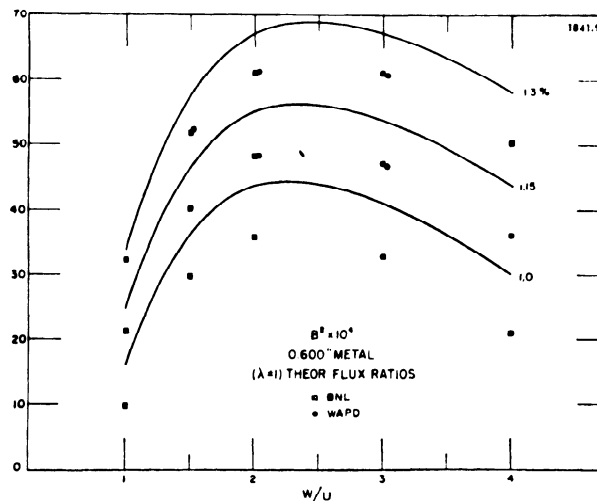


Figure 9. Multigroup and experimental values of B^2

yield second moments which are too small, the natural expectation is that the migration area computed here may account for the error. If the measurements of the migration area can be taken to indicate anything, they are in agreement with this surmise. On the other hand, this error in buckling represents an error in reactivity of less than 2% and it would be surprising if the errors in the calculation of other effects, such as resonance capture and thermal utilization, were not at least this large. Figure 9 shows the comparison.

Table 18. Delayed Neutron Effectiveness $\bar{\beta}_j/\beta_j$

Energy (kev)	$W/U = 2.0$	$W/U = 3.0$
250	1.032	1.057
560	1.004	1.031
430	1.015	1.042
620	0.998	1.026

An indication of enrichment dependent errors is found in the values of λ computed for the experimental buckling. In Table 16 it is seen that, in general, the values of λ increase as the enrichment of the system decreases. Any increase in migration area will tend to amplify this effect. The inclusion of rod size effect and aluminum inelastic scattering will tend to reduce the peak in λ at low W/U ratios, but should do so rather independently of enrichment. In overall effect, these last two corrections will tend to raise the general level of values of λ by a fraction of a percent above those quoted here.

Applicability to Two Regions

A strong test of the few group methods is their ability to predict the properties of multiregion systems. There is a set of measurements which sheds light on this matter and which makes the case for general applicability look quite good. This is a set of experiments done at Bettis with the TRX facility loaded with an inner region of oxide fuel elements of 0.383 in. diameter ($W/U = 4.9$) and an outer driving lattice of uranium metal rods of 0.387 in. diameter ($W/U = 2.4$). Measurements were done with two sizes of the sublattice, the first (91 fuel elements) providing an effective radius of 9.0 cm, and the second (37 elements) giving an effective radius of 5.8 cm.

For comparison, measurements were made in a uniform critical core with an effective radius of 37.6 cm containing 1575 fuel rods of the subregion material and geometry. Results found at the center of the sublattice were:

The experimental results can be compared with the predictions of calculations using a one dimensional, four group diffusion code. Radial flux values were obtained for fluxes of four average energies. The energy limits of the groups are as follows: group 1, from 10 Mev to 0.821 Mev; group 2, from 0.821 Mev to 5.53 Kev; group 3, from 5.53 Kev to 0.625 ev; group 4, from 0.625 ev to 0. The energy limits of group 1 were chosen to encompass the U²³⁸ fission range and those in group 3 to contain the resonance activation; group 4 is the thermal group. The calculated flux ratios ϕ_1/ϕ_4 , ϕ_3/ϕ_4 at the center of the lattice, normalized to the values for a full core made up entirely of the sublattice fuel, were:

Lattice	ϕ_1/ϕ_4	ϕ_3/ϕ_4
Full core (normalized)	1.000	1.000
9 cm inner radius	0.988	1.010
5.8 cm inner radius	1.009	1.059

ρ_{28} should be proportional to the ratio ϕ_3/ϕ_4 . The cadmium ratio should be proportional to the ratio $(1 + \phi_4/\phi_3)$. δ_{28} should follow the ratio ϕ_1/ϕ_4 . Within the experimental error, the data for both sublattices can be interpreted to agree with the calculations.

Table 19. Reduced Migration Area, Λ (cm²)

Rods	W/U	$d\lambda/dB^2$ (enrichment)	$d\lambda/dB^2$ (poison)
0.600 in.	1.15%	1	25.5
		1.5	28.5
		2	26.7
		3	26.0
		4	26.7
0.387 in.	1.3%	2	30.0 (water height)
		3	29.6 " "

Experimental and theoretical neutron activation plots for the 5.8 cm core are given in Figs. 10 and 11. The data were normalized to unity at the center of the reactor. The fast neutron plots were done with U²³⁸ foils and the slow flux plots were done with 1.3% U²³⁵ foils. For the subregion cores, activation plots were made along a corner of the hexagonal pattern as well as through the center of the sides. To compare the experimental activation with the calculations, it is necessary to multiply the calculated fluxes by the proper cross-sections to obtain an activation. In the case of the fast neutron activation plot, this is just $\Sigma_{f1}^{238} \phi_1$, where Σ_{f1}^{238} is the average macroscopic fission cross-section of U²³⁸ for group 1.

	δ_{28}	Cadmium ratio of U ²³⁵ (in fuel rod)	Cadmium ratio of U ²³⁵ (in moderator)	Average thermal flux ratio (water to fuel)	ρ_{28}
Full core	0.057 ± 0.001	19.1 ± 0.2	20.3 ± 0.2	1.13 ± 0.01	0.935 ± 0.02
9 cm inner radius	0.057 ± 0.001	19.4 ± 0.2	20.5 ± 0.2	1.12 ± 0.01	0.971 ± 0.02
5.8 cm inner radius	0.056 ± 0.001	18.6 ± 0.2	19.2 ± 0.2	1.13 ± 0.01	0.964 ± 0.02

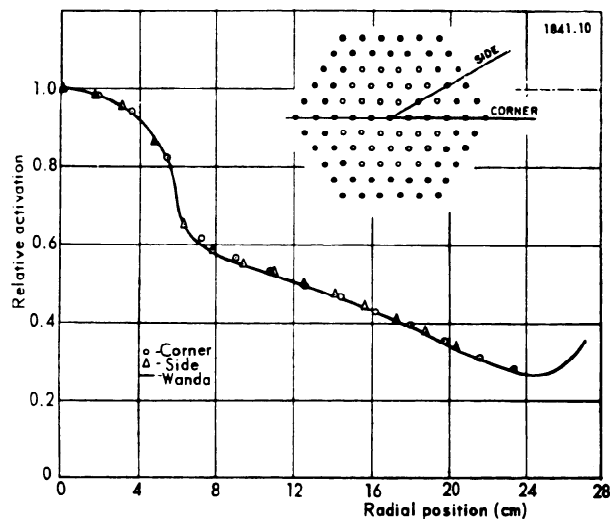


Figure 10. Thermal flux distribution in two-region lattice (5.8 cm inner region)

For a comparison with the 1.3% foils, the calculation becomes

$$\text{activation} = \sum_{i=1}^4 [\Sigma_{fi}^{25}\phi_i + \Sigma_{fi}^{28}\phi_i]$$

where the first term is the product of the U^{235} macroscopic fission cross-sections and the appropriate calculated flux values, and the second contains the macroscopic fission cross section of the U^{238} in these foils. The cross sections used in these calculations for the first three groups were obtained using MUFT-III; the group 4 cross sections (thermal region) were obtained from SOFOCATE.

The slow neutron activations agree very well with the calculated values. The fast neutron activations agree very well with the calculations in the outer region of the metal but do not agree in the inner region near the boundary. Here, the experimental

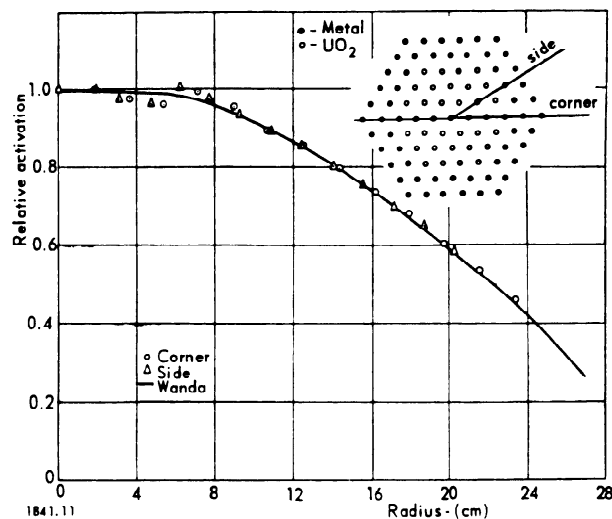


Figure 11. Fast flux distribution in two-region lattice (5.8 cm inner region)

points show a marked dip and peak which is not shown by the calculations and which has been shown to be caused by the inability of the latter to follow the rapid change occurring at the boundary.

The close agreement of measurements and calculations of sublattice properties is most encouraging, and can be considered as an excellent experimental basis for using the few group method with multi-region geometries.

Moreover, the agreement implies that the few group calculations can be used as reliable guides to the worth of data obtained in small assemblies, such as these sublattices. With such a guide available, it now becomes possible to make extensive experimental parametric surveys of the properties of reactor cores, using sublattices inside a driving lattice of another composition. A considerable saving in needed fuel will thereby be realized.

APPENDIX 1

Table 20. Lattice Geometry

Lattice designation Fuel	W/U	Enrichment weight %	Dimensions		W/U	Volume ratios	
			X (cm)	r _c (cm)		Al/U	W/UO ₂
U metal	1.5		2.404	1.263	1.515	0.198	
1.3%, 0.600 in.	2	1.294	2.616	1.374	2.017	0.198	
	3		2.990	1.570	3.011	0.198	
U metal	2		2.616	1.374	2.017	0.198	
1.15%, 0.600 in.	3	1.145	2.990	1.570	3.011	0.198	
U metal	2		1.725	0.906	2.024	0.318	
1.3%, 0.387 in.	3	1.296	1.961	1.030	3.018	0.318	
UO ₂ , 7.53 gm/cm ³	3		2.205	1.158	3.048	0.198	1.071
1.3%, 0.601 in.	4	1.311	2.359	1.239	4.000	0.198	1.405
	5		2.512	1.319	5.000	0.198	1.756
UO ₂ , 7.52 gm/cm ³	4		1.558	0.818	3.953	0.317	1.386
1.3%, 0.388 in.	5	1.311	1.652	0.868	4.947	0.317	1.734
UO ₂ , 10.53 gm/cm ³	3		1.558	0.818	2.904	0.324	1.426
1.3%, 0.383 in.	3.6	1.311	1.652	0.868	3.622	0.324	1.779
	5		1.806	0.948	4.878	0.324	2.396

Symbols: X Distance between adjacent fuel rod centers.
 r_c Radius of a circle of area equal to the unit cell area.
 Al Aluminum.
 W Water
 U Total uranium (density 18.9 gm cm³).

APPENDIX 2. INHOUR FORMULA

The following formula has been used to calculate the reactivity corresponding to a measured reactor period T .

$$\rho = \beta^{235} I \sum_{i=1}^6 \frac{1 + \frac{(\beta\nu)^{238} a_i^{238}}{(\beta\nu)^{235} a_i^{235}}}{1 + \frac{\nu^{238}}{\nu^{235}} \delta_{28}} \cdot \frac{a_i^{235}}{1 + \lambda_i T}$$

- where T is the reactor period in seconds.
 λ_i is decay constant of i th delayed neutron group.
 a_i is the yield of the i th delayed neutron group normalized such that $\sum a_i = 1$. Superscript represents the yield from either U²³⁵ or U²³⁸ fissions.
 $\beta\nu$ is the total delayed neutron yield per fission of either U²³⁵ or U²³⁸.
 ν is the number of prompt neutrons per fission for either U²³⁵ or U²³⁸; we have used $\nu^{235} = \nu^{238} = 2.47$.
 δ_{28} is the ratio of U²³⁸ fissions to U²³⁵ fissions in the lattice. This number is experimentally obtained for each lattice and is listed in Table 21.
 I is a quantity expressing the ratio of the "importance" of delayed neutrons to prompt neutrons in the fission cycle. It is calculated using a multigroup computer code and the delayed neutron group energy obtained from Table 18. This importance is a function of the reactor period but changes only by about $\frac{1}{10}$ of 1 per cent over the range of periods used (80 to 5000 sec) in the present measurements. The values of I calculated for each lattice are shown in Table 21.

Table 21. Inhour Formula Parameters used in Analysis of Kinetic Experiments

Lattice designation Fuel	W/U	Ratio of U ²³⁸ fissions	Relative importance of delayed neutrons, I
U metal	2	0.109 ± 0.002 ^a	1.024
1.3%, 0.600 in.	3	0.084 ± 0.002 ^a	1.043
U metal	2	0.104 ± 0.015 ^b	1.006
1.15%, 0.600 in.	3	0.081 ± 0.012 ^b	1.024
U metal	2	0.099 ± 0.015 ^b	1.014
1.3%, 0.387 in.	3	0.078 ± 0.012 ^b	1.043
UO ₂ , 7.53 gm/cm ³	3	0.071 ± 0.010 ^b	1.034
1.3%, 0.601 in.	4	0.059 ± 0.009 ^b	1.045
	5	0.051 ± 0.004 ^b	1.046
UO ₂ , 7.52 gm/cm ³	4	0.063 ± 0.003 ^b	1.039
1.3%, 0.388 in.	5	0.054 ± 0.003 ^b	1.040
UO ₂ , 10.53 gm/cm ³	3	0.078 ± 0.004 ^b	1.030
1.3%, 0.383 in.	3.6	0.070 ± 0.004 ^b	1.042
	5	0.057 ± 0.003 ^b	1.044

^a Ref. 1.

^b Ref. 5.

16

The six delayed neutron group parameters of Keepin *et al.*¹³ are used in the inhour equation.

APPENDIX 3. WORK WITH UO₂ ENRICHED TO 4% U²³⁵

In conjunction with the fulfilment of the Nuclear Merchant Ship contract with the United States Atomic Energy Commission, a series of critical experiments have been performed by the Babcock & Wilcox Company (USA) with uranium enriched to 4% U²³⁵. These experiments were performed in configurations similar to the power core design and in unperturbed lattices.

Fuel Element Description

The basic fuel unit is the fuel pin. Each pin contains 1600 grams (± 5 grams) of UO₂ powder compacted to an average density of 9.45 g/cm³ (± 0.1 g/cm³). The average assay is 4.02% U²³⁵/U_{total}, by weight, and the average uranium content is 0.880 U/UO₂.

Figure 12 shows the pin dimensions, lattice spacing, and a sketch of the can element. Table 22 lists water-to-uranium-metal ratios (W/U), computed according to the definition in the main body of this paper, and water-to-uranium-oxide volume ratios (W/UO_2). All work was done with oxide lattices.

Core Descriptions

With the exception of Core V, the configurations tested all included can walls (stainless steel or aluminum) and water gaps between cans for the inclusion of control blades or blade followers. Two lattice spacings were used for each of the two can wall materials. Figure 13 includes a sketch of the spacings around a can.

Criticality

Figure 2 shows the critical configurations for each of the 4% cores tested. The excess reactivity (quoted in cents) is for the clean core condition with nothing in the blade channels but water.

Water Height Measurements

In each of the cores, measurements were made of the change in reactivity (as measured by positive periods) as a function of water height. As discussed in Refs. 6 and 15, this can be related to migration area and infinite medium multiplication, although the exact form depends on the model chosen to express the non-leakage probability.

$$C = \frac{1}{k_{\infty}} \frac{\partial P^{-1}}{\partial B_z^2} = \frac{(h+\lambda)^3}{2\pi^2} \frac{\partial \rho}{\partial h} \quad (33)$$

Equation 33 assumes that k_{eff} is $k_{\infty} P(B^2)$ the infinite medium multiplication times the non-leakage probability and that the vertical buckling, B_z^2 , can be written as $\pi^2/(h+\lambda)^2$, where h is the core height. For the case of partial water height, h is the distance from the bottom active fuel line to the top water

1841.12

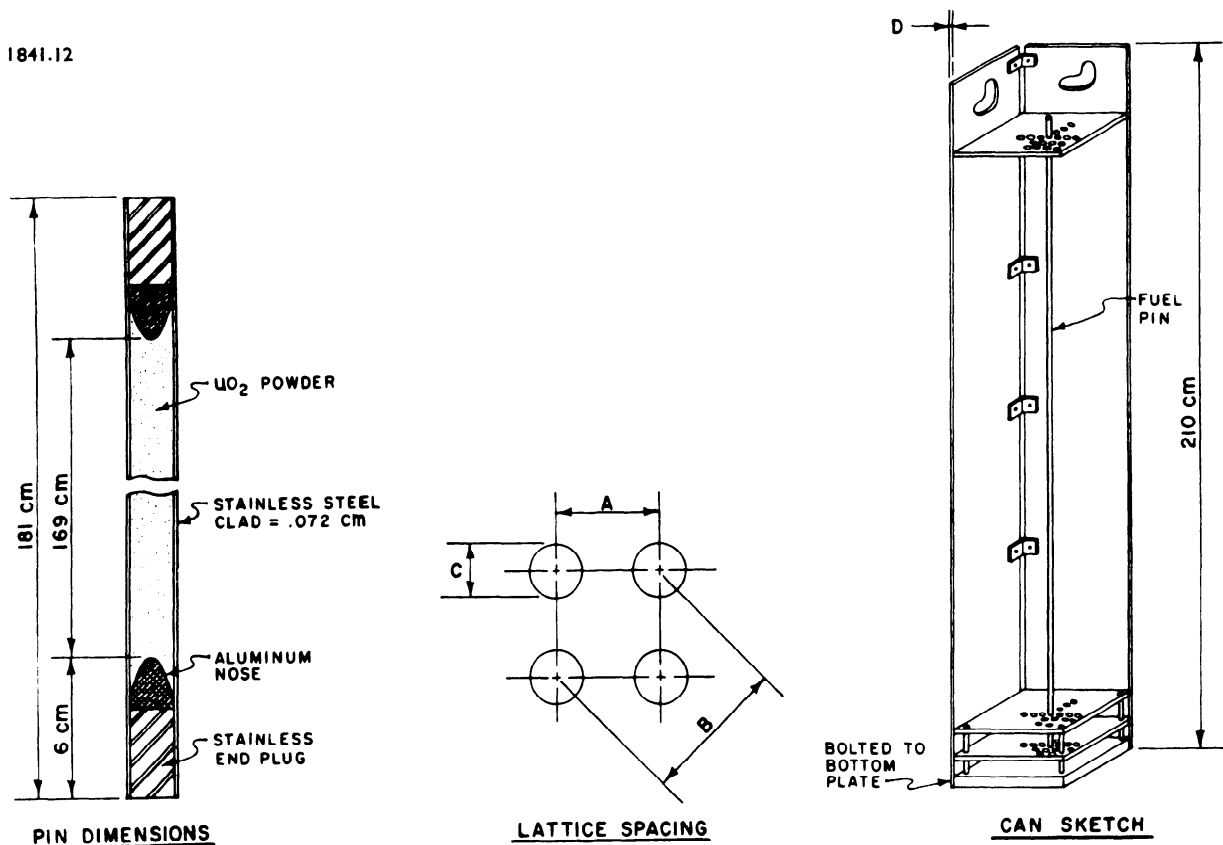


Figure 12. Experimental details

surface. The λ is the vertical reflector savings. It has been found experimentally that this reflector savings is constant if the surface of the water is at least 30 cm below the top active fuel line. The reactivity, ρ , is expressed in dollars and has been related to the period through a multigroup inhour formula¹³ with the inclusion of the effect of delayed neutrons from the fast fissions of U^{238} . Because the effective delay fraction depends upon the fast effect and on the leakage probability ratio between prompt neutrons and delayed neutrons, there is a change in delayed neutron effectiveness between cores with different critical bucklings. As discussed later, the difficulty in determining the bucklings of cores including water gaps and can walls has not permitted reliable determination of M^2 and k_{∞} except for the "clean" Core V. Figure 14 shows a typical plot of the water height data, and Table 23 gives the constants determined from the cores measured.

B^2 , M^2 , k_{∞} Determinations

Material bucklings for the critical configurations were based on two methods; (1) J_0 and cosine fit of flux maps and (2) the assumed constancy of critical buckling and reflector savings as the water height is reduced and the radius increased. Both methods give an average number which combines the effect of lattice leakage due to the core boundaries and leakage into the water gaps from the individual cans. Table 24 gives the experimental parameters for the "clean" Core V. The vertical reflector savings was determined for full and for partial water height where the top reflector is a forest of dry fuel pins at least 30 cm long. The table shows buckling determinations by both flux plots and partial water height data.

For the case of Core V, the buckling data has been used to separate M^2 and k_{∞} . The effective delay

Table 22. Core Constants

Core No.	A (cm)	B (cm)	C (cm)	D (cm)	Can wall mat'l	W/UO_2	W/V
I	1.685	2.383	1.270	0.398	304-SS	1.544	3.51
II	1.555	2.197	1.270	0.398	304-SS	1.147	2.60
III	1.555	2.197	1.270	0.330	6061-AL	1.147	2.60
IV	1.685	2.383	1.270	0.330	6061-AL	1.544	3.51
V	1.685	2.383	1.270	—	No cans or gaps	1.544	3.51

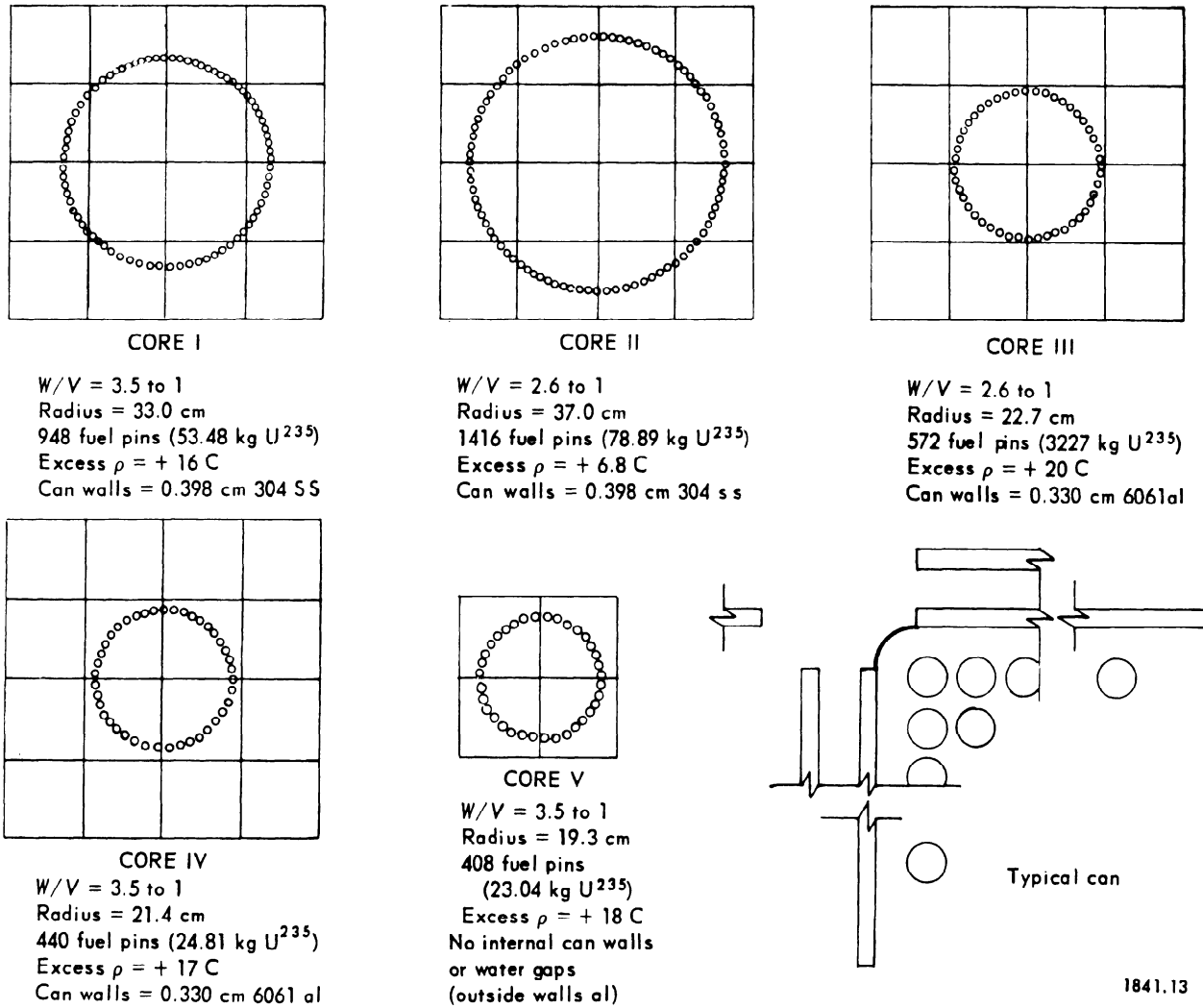


Figure 13. Critical configuration of 4% enriched cores

fraction has been computed from the one-group leakage model. The migration area of delayed neutrons for this core taken from Multigroup Code similar to MUFT III is 0.35 the migration area of prompt neutrons.

$$\gamma = \frac{1 + M^2 B_c^2}{(1 + f M^2 B_c^2) \epsilon} \quad (34)$$

ϵ = fast effect
 B_c^2 = critical buckling
 M^2 = migration area of fission neutrons

$$M^2 = \frac{\gamma \beta C}{1 + \gamma \beta C B_c^2} \quad (35)$$

β = delayed neutron fraction

$$k_{\infty} = \frac{1}{1 + \gamma \beta C B_c^2} \quad (36)$$

f = ratio of migration area delayed neutrons to fission neutrons

The values tabulated in Table 24 are for the case of the one-group leakage model. The value for β includes effects of U²³⁸ fissions (5.9% of total).

Temperature Effects on Reactivity

On Cores I and II, the isothermal temperature effect on reactivity was determined between room temperature and 60°C. The results are shown in the

two graphs of the coefficient vs. temperature in Fig. 15. In each case, the gaps between cans were filled with blades or followers except for the channel used for cocked safety blades. The pattern is shown with the figure.

The initial positive coefficient has been predicted

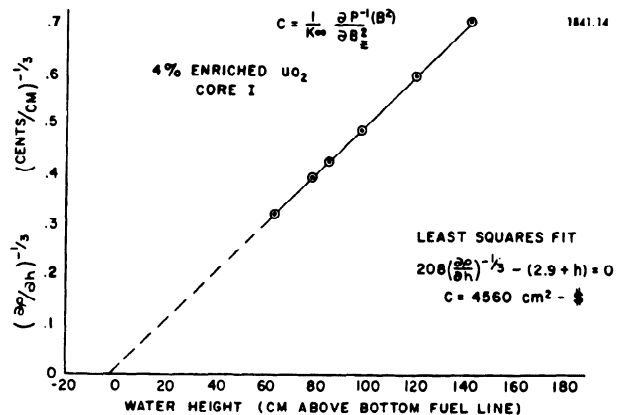


Figure 14. Determination of C

Table 23. Experimental Parameters, 4% UO₂ Cores

Core	C(cm ² -§)	γ	βγ	M ² /k _∞ (cm ²)	B _c ² (from flux maps)	B _c ² (constant reflector savings)
I	4560	1.053	0.00723	33.0	35.3 × 10 ⁻⁴ cm ⁻²	35.9 × 10 ⁻⁴ cm ²
II	5421	1.039	0.00732	39.7	26.7	26.7
III	5704	1.147	0.00801	45.7	61.0	51.1
V	3772	1.185	0.00826	31.4	85.6	86.6

on the basis of the large peaking of thermal flux through the can walls and adjacent water gaps. In both cases, the coefficient becomes negative at relatively low temperatures.

Table 24. Core V Parameters, 4% Clean Lattice

B_{critical}^2 (flux fits) = 85.6 × 10 ⁻⁴ cm ⁻²
B_{critical}^2 (constant savings) = 86.6 × 10 ⁻⁴ cm ⁻²
β (total delay fraction) = 0.00698
γ (effectiveness factor) = 1.16
βγ (effective delay fraction) = 0.00810
$C \left(\frac{1}{k_{\infty}} \frac{\partial P^{-1}}{\partial B_z^2} \right) = 3772 \text{ cm}^2 - \text{§}$
M ² /k _∞ (one group) = 30.88 cm ⁻²
M _P ² = 41.54 cm ²
k _∞ = 1.360
λ _H (full water height) = 5.04 cm
λ _H (partial water height) = 9.64 cm
λ _R (radial) = 6.53 cm

Cadmium Ratios and Disadvantage Factors

Figure 16 shows schematically the foil arrangements for measurements of thermal flux and cadmium ratios within the lattice of Core I. Dysprosium-aluminum alloy sector foils (5% by wt Dy) were used to determine the thermal flux, and the cadmium ratio in the water was measured as 22.

Table 25 lists the disadvantage factors in Cores I and II. The thermal flux ratios shown in this table were determined after correcting for sector volume and weight of the foils. The thermal utilization *f*, tabulated in the figure is the thermal absorptions in U²³⁵ per total thermal absorption in the core.

Interpretation of the cadmium ratios can be based on the modified two-group model which separates the infinite multiplication into two parts; the "fast" multiplication, "k₁", which is the number of neutrons produced epi-thermally per total produced and thermal multiplication *k*₂, which is the number produced thermally per total. For experimental convenience, the dividing energy is the cadmium cut-off near 0.4 ev.

Control Blade Worths and Integral Water Height and Determinations of *k*_{eff}

As shown in Fig. 17, the differential water worth of a given core (e.g., Core II) is approximately in-

dependent of whether the increased water height was balanced by changing the radius of the core or by the insertion of control blade material in the water gaps between cans. Control blades were cross shaped, 20.3 cm tip to tip, ¼ in. boral.

This has made possible the evaluation of control blade patterns for their effectiveness in holding the reactor critical and comparison of different cores for the total *k*_{eff} being held down by blades.

The integration of the differential water worth curve (numerically, by Simpson's rule) provides a water worth curve in dollars. The excess reactivity in dollars can then be read for the just critical water height for any blade pattern. The conversion to *k*_{eff} is then done with the delay fraction appropriate to the full size core; that is, with the water fully raised.

In Core III, the value of the central blade as a function of radius was determined and is shown in Table 26. The value of the blade was approximately inversely proportional to the effective radius squared.

APPENDIX 4. MEASUREMENTS ON A LATTICE OF STAINLESS STEEL CLAD SLIGHTLY ENRICHED URANIUM DIOXIDE FUEL RODS IN LIGHT WATER

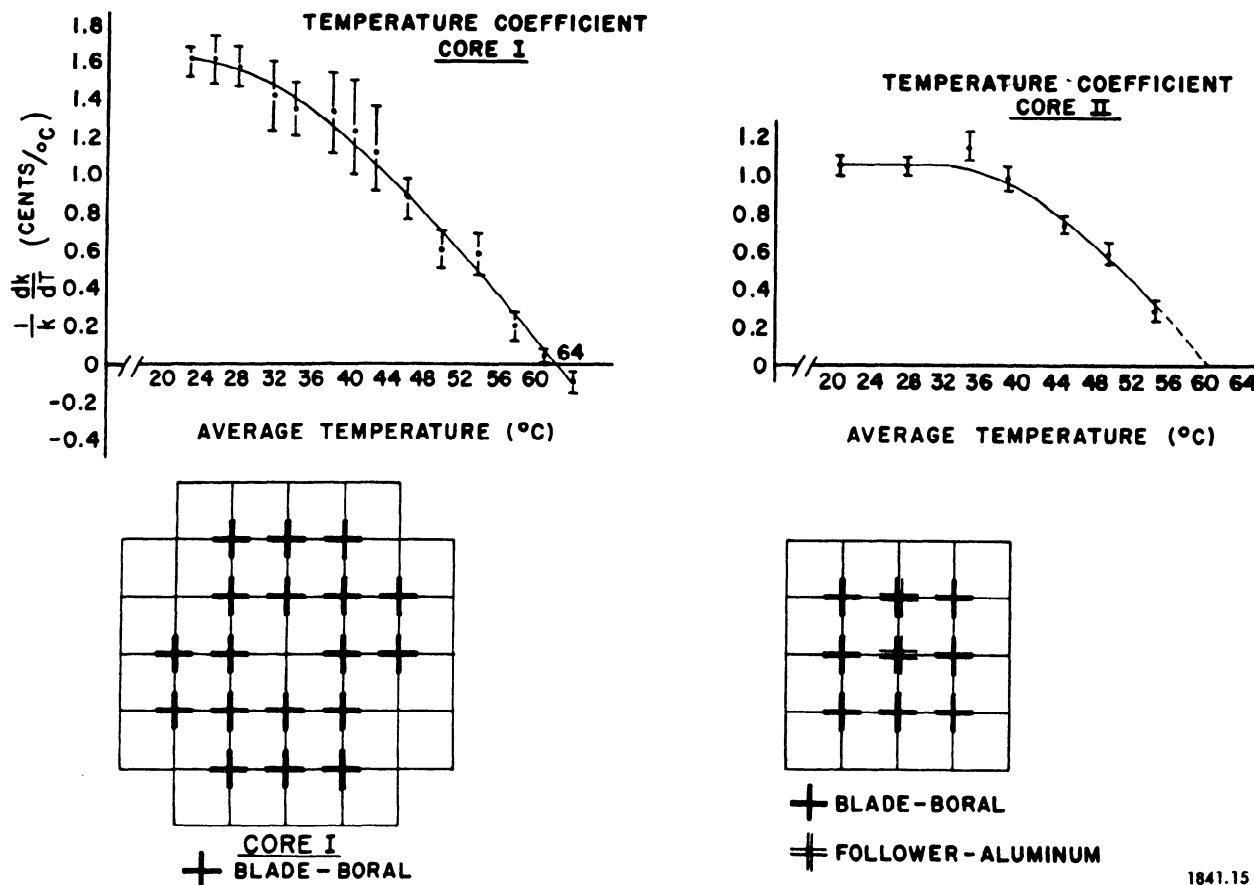
As part of the research and development program for the design of the Yankee Atomic Electric Power Reactor¹⁷ by the Westinghouse Atomic Power Department, a series of critical experiments is being conducted at the Westinghouse Reactor Evaluation Center. The design of the reactor used in these experiments is based on the reference design of the power

Table 25. Disadvantage Factors in Lattice—Core I and II

Core No.	φ _{UO₂}	φ _{SS}	φ _{H₂O}	<i>f</i> ₂₅
I	1	1.10	1.43	0.758
II	1	1.19	1.29	0.770

Table 26. Central Blade Worth vs. Radius—Core III

No. pins	Effective radius, cm	Central blade worth, §	(Radius) ² × worth / 1000
2384	47.1	4.02 ± 0.20	8.90
1944	42.8	4.83 ± 0.30	8.85
1344	36.0	6.96 ± 0.50	9.00



1841.15

Figure 15. Reactivity temperature coefficients

reactor and is a thermal reactor having stainless clad, 2.7 weight percent enriched uranium dioxide sintered pellet fuel rods, moderated and reflected with ordinary water.

The purpose of these critical experiments is twofold: to furnish reactor physics parameters and to test analytical methods which are to be used in connection with the nuclear design of the core for the power reactor. The complete series of experiments will include measurements of critical size; buckling and reflector savings; migration area; disadvantage factor; temperature coefficient; void coefficient; control rod worths and interactions; and flux distributions with partially inserted control rods, through water gaps and through regions containing stainless steel straps. Certain of these measurements are being made with a poisoned moderator containing boric

acid as well as with a clean moderator. Also, the measurements will be made for three (water)-to-(contained uranium metal) volume ratios; 3.03 : 1, 2.23 : 1 and 3.81 : 1. However, the results reported here are concerned only with the critical size, the buckling and the central control rod worth for the clean core with the 3.03 : 1 ratio.

Description of the Reactor

The Yankee Critical Experiments Reactor is a "zero power" thermal reactor having stainless steel clad, slightly enriched uranium dioxide pellet fuel elements moderated and reflected by ordinary water. This reactor was designed by the Reactor Engineering Department of the Westinghouse Atomic Power Department. It has been installed in the Westinghouse Reactor Evaluation Center, located near the

1841.16

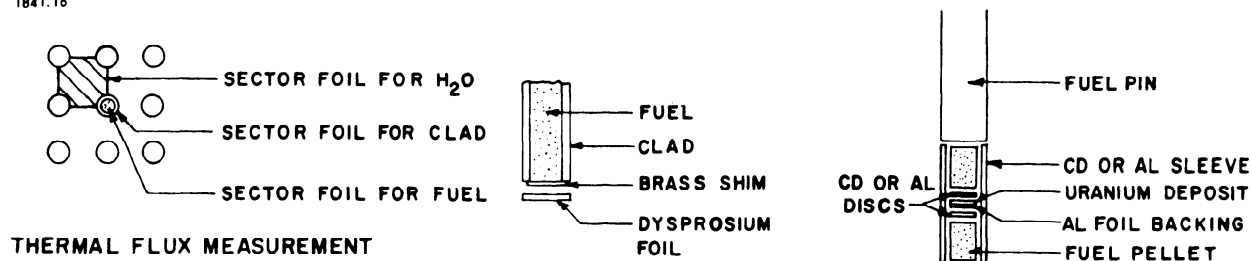
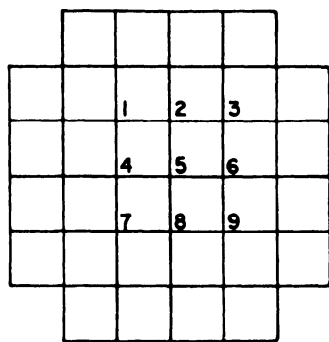
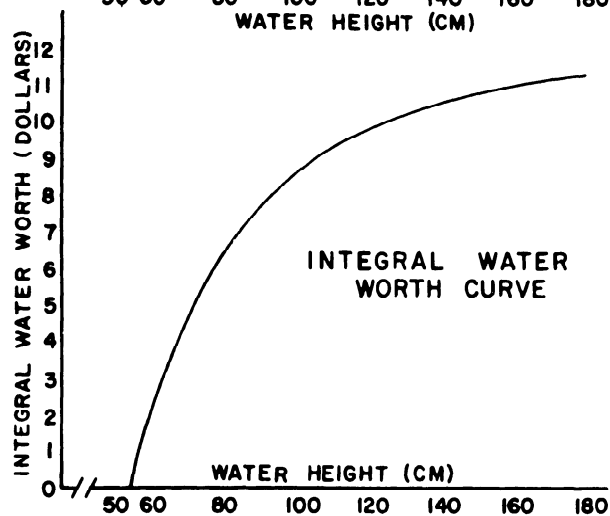
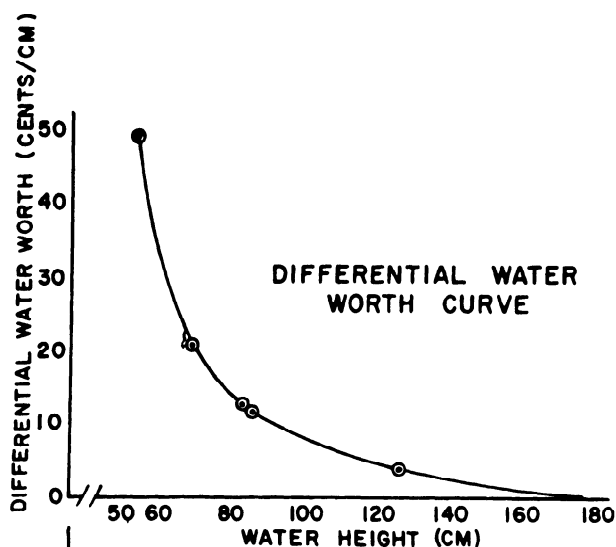


Figure 16. Fuel pin details



	ρ_{ex}	K_{eff}
NO BLADES	11.20	1.093
CENTRAL BLADE NO. 5 ONLY	10.10	1.083
CENTRAL 9 BLADES	3.95	1.031
ALL BLADES IN	-5.00	.961

1841.17

Figure 17. Water worth curves

village of Waltz Mill, Pennsylvania. It first went critical on December 18, 1957.

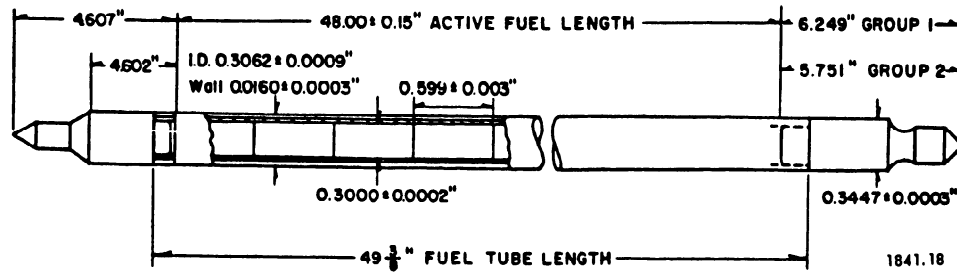
The fuel elements for the Yankee CRX Reactor are in the form of single rods containing 2.7 weight percent enriched sintered uranium dioxide pellets sealed in Type 304 stainless steel tube cladding. The properties of the fuel and the cladding are summarized in tabular form in Fig. 18, where the assembly of a fuel rod is also indicated. All except 50 of the fuel rods are sealed at both ends by stainless steel end plugs which are welded in place. The remaining 50 fuel rods have removable end plugs and are sealed with double "O" rings.

The fuel rods are held vertically in their lattice configuration by means of four core plates. These plates contain an array of holes drilled in a square pattern as indicated in Fig. 19. The holes have a center-to-center spacing of 0.435 in. which defines the (water)-to-(contained uranium metal) volume ratio of the reactor as 3.03 to 1. The top core plate is one inch thick aluminum and the bottom plate is one and one half inch aluminum. The other two plates are made of one-half-in.-thick lucite and are located at one-third and two-thirds of the distance between the top and bottom plates. These plates are held in position by means of a cylindrical aluminum core barrel as shown in Fig. 20.

As indicated in Fig. 19, the core plates also have nine cruciform slots to accommodate the control rods. Each of these slots, when in the effective portion of the core, displaces a maximum 37 fuel rods. However, provision has been made whereby the slots not occupied by control rods can be filled with fuel to give a more uniform core. Figure 21 is a photograph of the top of the reactor showing two control rods in place, the central slot filled and two outer slots partially filled with fuel. This core, which was slightly supercritical when the control rods were withdrawn, contained 1839 fuel rods.

The control rods for the Yankee CRX reactor have a cruciform cross section with a span of 7.812 ± 0.010 in.; a thickness of 0.285 ± 0.003 in. and an overall length of 112.5 in. The poison portion of the rod is 48 in. long. Above it is a 11.375 in. long Type 304 stainless steel coupling section and below it is a 53.875 in. long aluminum follower. Both of these overlap the poison section by 0.375 in. as part of the joining design. The poison section consists of 69.83% silver, 30.15% cadmium with 0.02% zinc, less than 0.1% copper and only slight traces of other elements.

The control rods are coupled by means of rigid shafts to rack and pinion type drive mechanisms. They can be withdrawn one at a time at a speed of six in. per minute. They can be inserted singly or in a group at six in. per minute. For fast insertion, they can be dropped individually or as a group under the action of gravity by disengaging the magnetic clutches which are located on the pinion drive shafts. The maximum travel of the control rods is 48 in. 122 cm, and in the fully withdrawn position, the poison section ends at the top of the fuel.



Fuel		Dimensions		Cladding	
Enrichment	2.700 ± 0.017 Wt/100	Type		304 stainless steel	
Form	Sintered UO ₂ pellets	Tubing			
Pellets/rod	80	Inside diameter	0.3062 ± 0.0009 inch		
Diameter	0.3000 ± 0.0002 inch	Wall thickness	0.0160 ± 0.0003 inch		
Length/pellet	0.5989 ± 0.0034 inch	Length	49.420 ± 0.007 inches		
Length/rod	47.997 ± 0.150 inches	Weight	104.45 ± 1.35 grams		
Density/pellet	10.71 ± 0.19 g/cm ³	End plugs			
Weight/pellet	7.07 ± 0.13 grams	Long		Short	
Weight/rod	566.04 ± 4.58 grams	Diameter	0.3447 ± 0.0003	0.3447 ± 0.0003 in.	
		Length	6.2487 ± 0.0006	5.7510 ± 0.0003 in.	
		Weight	70.43 ± 0.09	64.41 ± 0.09 grams	

Fuel		Chemical analysis		Cladding	
Element	Percent or parts per million	Element	percent		
U	88.7%	C	0.06		
UO ₂	99.2%	Mn	1.23		
C	0.008%	P	0.03		
E	25 ppm	S	0.015		
Fe	617 ppm	Si	0.50		
Mo	2 ppm	Ni	9.58		
B	<0.5 ppm	Cr	18.20		
Cu	2 ppm	Mo	0.23		
Pb	2 ppm	Cu	0.35		
Cr	63 ppm	Fe	Remainder		
Sm	1 ppm				
Ag	<0.1 ppm				
Ni	80 ppm				
Si	19 ppm				

Figure 18. Yankee CRX fuel rods

The reactor core structure is mounted in a stainless steel tank six ft in diameter and seven ft high as indicated in Fig. 20. The tank has a bottom extension four ft in diameter by four ft deep to accommodate the follower sections of the control rods. The start-up source, also located in this extension tank, can be moved by means of a four-ft long lead screw drive to and from its start-up position just under the center of the bottom core plate. It is a one curie (1.4 × 10⁶ n/sec) plutonium-beryllium source and has been found very satisfactory for start-up purposes.

The water used as a moderator and reflector is ordinary tap water which has been passed through a mixed bed, amberlite, ion-exchange resin demineralizer. The specific resistance of the water is maintained at greater than 500,000 ohm-cm.

Critical Size

The determination of the clean critical size of the Yankee CRX reactor is complicated by the fact that the control rods and/or their aluminum followers displace fuel. This means that the reactor can never be made perfectly "clean". Under the best conditions,

two control rod followers were in the core. However, it has been possible to extrapolate to the "clean" condition by determining the critical size with first four and then two control rod followers in the core. The difference between the two values thus obtained represents the reactivity effect of two of the followers. The values obtained are presented in Table 27 below.

A correction has been applied to compensate for the slight amount of excess reactivity in the cores actually measured. The control rod locations are identified in Fig. 19.

Critical Buckling

The critical buckling, B^2 , for the Yankee CRX reactor was obtained by experimentally determining the radial and axial buckling, that is, by measuring the quantities in the expression

$$B^2 = B_g^2 = B_r^2 + B_h^2 = \left(\frac{2.405}{R + \lambda_r} \right)^2 + \left(\frac{\pi}{H + 2\lambda_h} \right)^2 \quad (37)$$

where B_g^2 is the geometrical buckling
 B_r^2 is the radial buckling

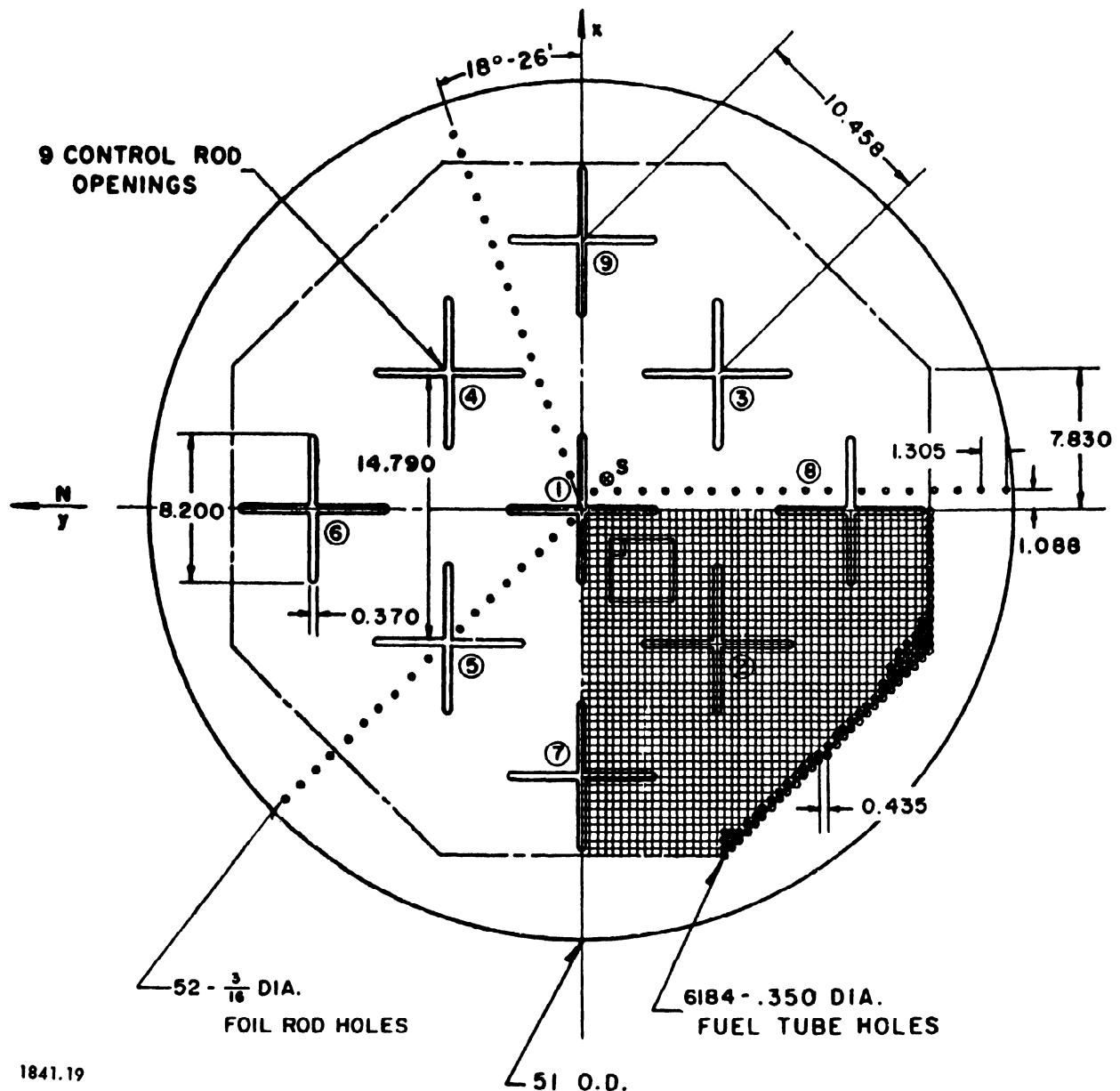


Figure 19. Yankee CRX core plate ratio 3.03 : 1

- B_h^2 is the axial buckling
 R is the actual core radius
 H is the actual core height
 λ_r is the radial reflector savings or extrapolation length
 λ_h is the axial reflector savings or extrapolation length

The actual core radius was found by determining the clean critical size and using the relation:

$$R^2 = \frac{\text{horizontal core area}}{\pi} = d^2 N / \pi \quad (38)$$

where d is the center-to-center distance between fuel rods and N is the number of fuel rod spaces filled including those occupied by control rods and/or their followers.

As discussed previously, the number of fuel rods for the clean critical core was found to be 1849 ± 1 . The center-to-center distance between fuel rods is 1.105 cm with a tolerance of ± 0.013 cm between any two fuel rods. Thus, the radius, R , is 26.80 ± 0.04 cm. The actual height was measured for each fuel rod and the standard deviation obtained giving $H = 121.9 \pm 0.4$ cm.

The radial and axial reflector savings were obtained by the standard technique of measuring the radial and axial neutron flux distributions and then fitting them to the appropriate analytical curves. The neutron flux distributions were measured by two different methods. One method involved the activation of gold or indium foils or copper wires placed between fuel rods along a diameter or near the axis of the reactor. Then the specific activity of each foil

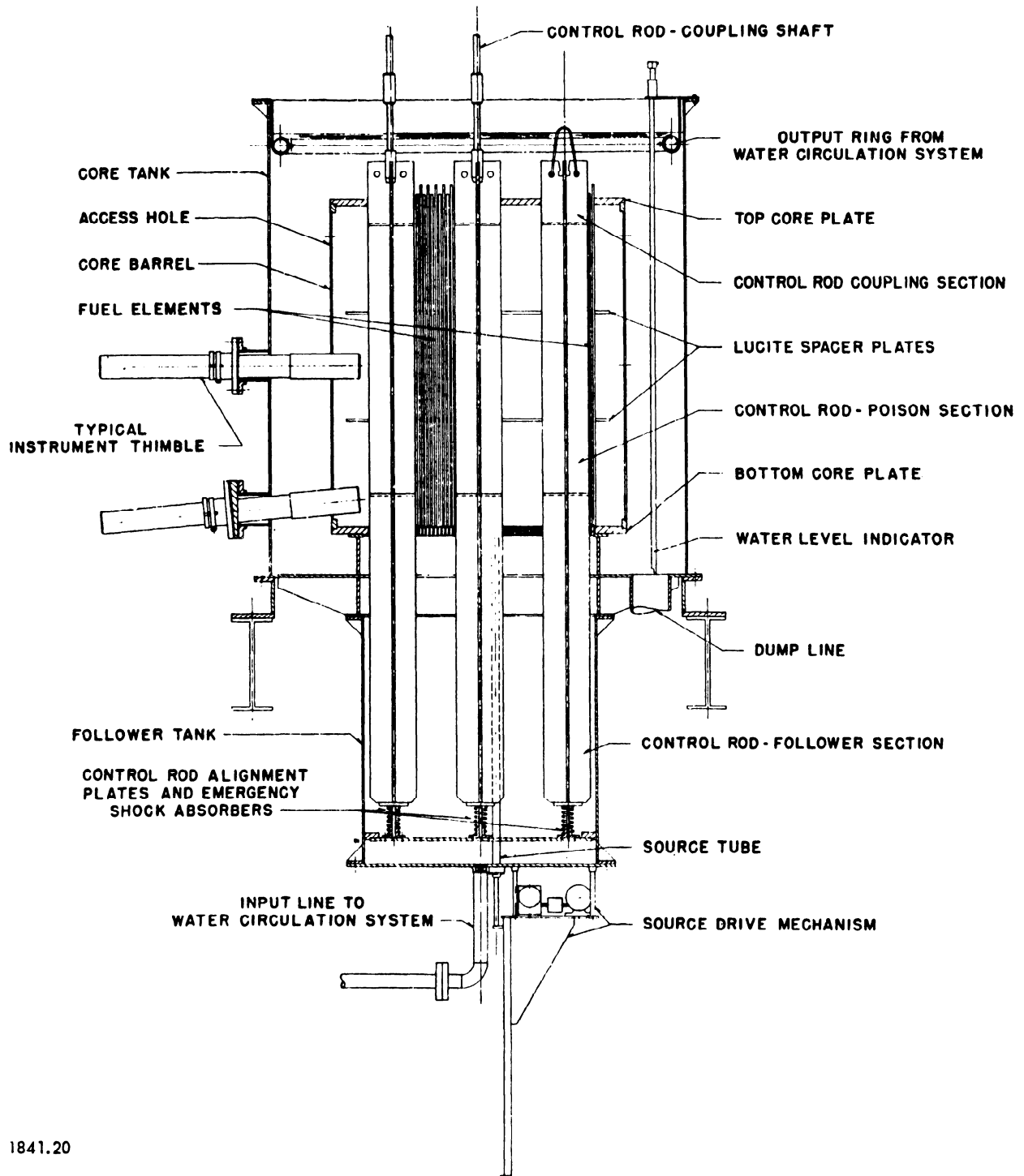


Figure 20. Vertical cross section of Yankee CRX core and core tank

1841.20

Table 27. Critical Size, Yankee CRX Reactor

 $W/U=3.03$; Cylindrical Configuration 121.9 cm high; Temperature = 13°C

Control rod locations	Number of fuel rods	Radius cm	UO_2	Mass (kilograms) U	U^{235}
2, 3, 4 and 5	1825	27.18 ± 0.04	1033 ± 8	916 ± 8	2.47 ± 0.02
3 and 5	1837	26.99 ± 0.04	1040 ± 8	922 ± 8	2.49 ± 0.02
None (extrapolated)	1849 ± 1	26.80 ± 0.04	1047 ± 8	928 ± 8	2.51 ± 0.02

or section of wire was found by measuring the beta-ray activity with end-window Geiger counters and applying the appropriate correction factors. The second method involved the measurement of the fission product activity induced in individual fuel rods irradiated in the reactor. To obtain axial flux distributions, the activity was measured along the length of fuel rods from near the center of the reactor. To obtain radial flux distributions, the activity was measured at a given height on a series of fuel rods which had been located along a diameter of the reactor. The fission product activity was determined

by gamma-ray counting with a NaI(Tl) scintillation counter biased to count all gamma-rays with energies over 0.5 Mev. The crystal and photomultiplier were mounted in a lead shield with a 0.50 in. wide slit. The fission product decay correction was made automatically by using the activity of a fixed fuel rod in a monitor channel to time the counting interval of the data channel. This correction was checked by repeating data counts at regular intervals.

The flux distribution data were then least-squares fitted to a zero order Bessel function of the first kind for the radials or a Cosine function for the axial

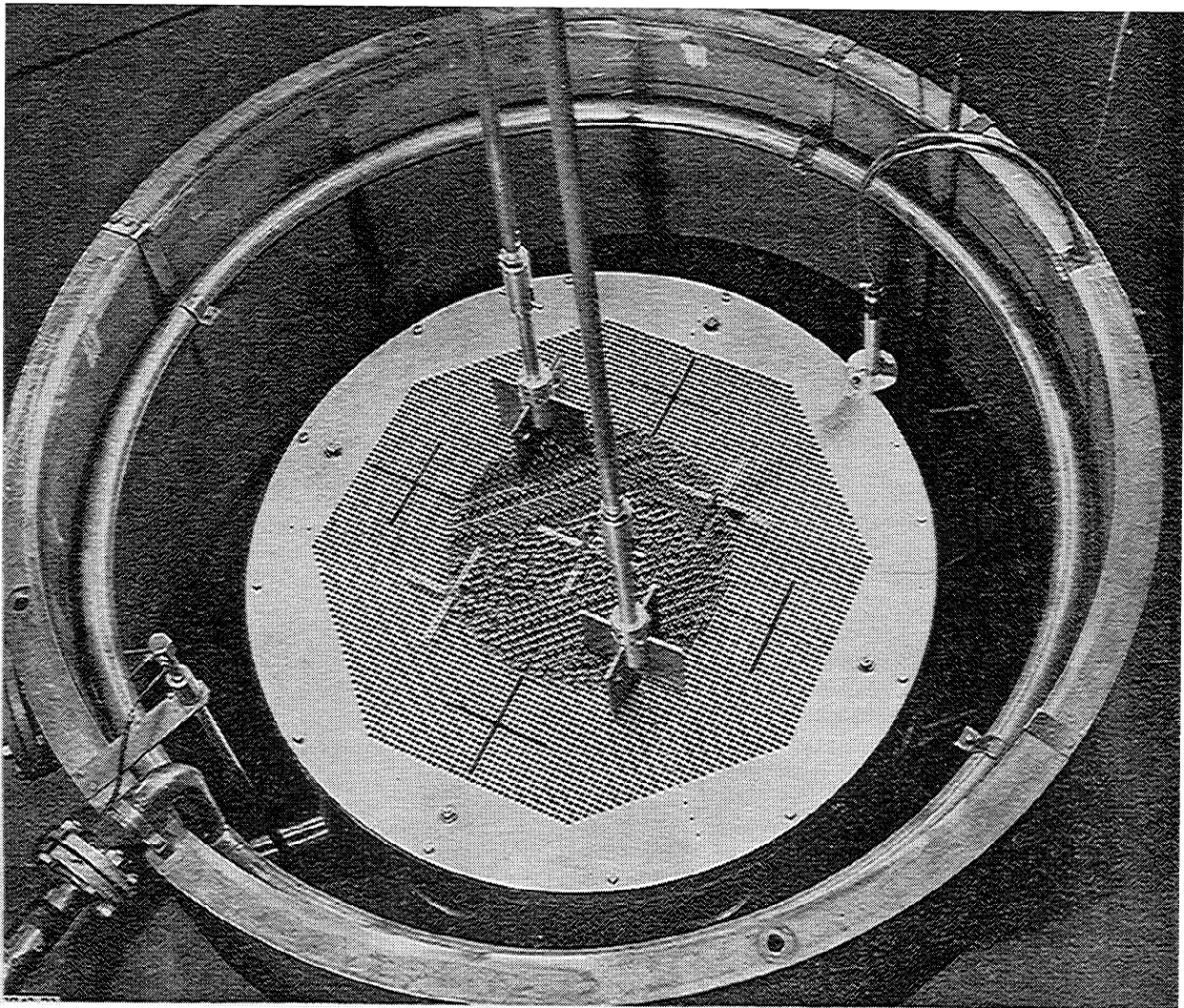


Figure 21. Yankee CRX reactor—top view of 3.03 : 1 core

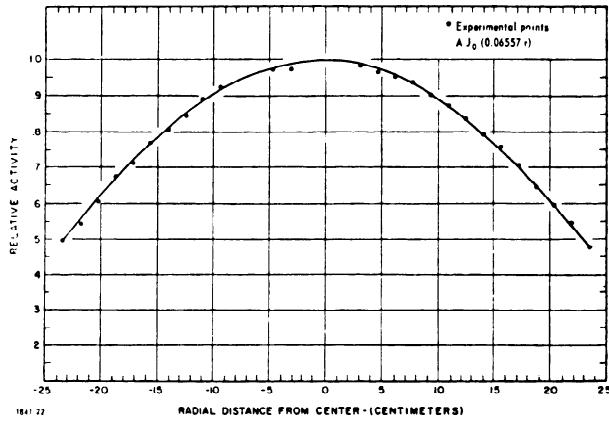


Figure 22. Radial flux distribution—Yankee critical experiments—3 : 1 core (by fuel rod scanning technique); actual radius = 29.36 cm; $\lambda_r = 7.31 \pm 0.16$ cm

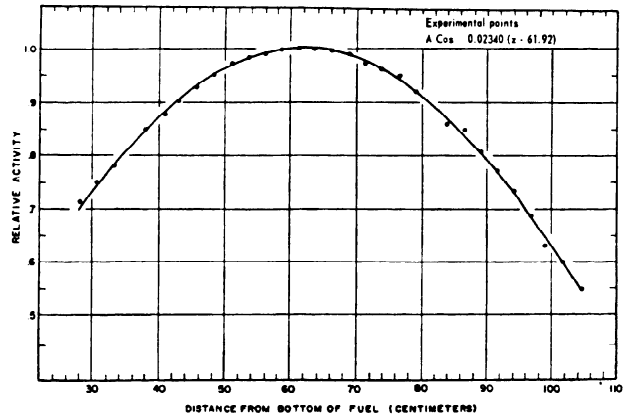


Figure 23. Axial flux distribution—Yankee critical experiments—3 : 1 core (by fuel rod scanning technique); actual height = 121.9 cm; $\lambda_h = 6.2 \pm 0.3$ cm

measurements. This was done by means of codes set up for the IBM-704 computer. These codes calculate the buckling, the extrapolated core radius or height and the center shift as well as the standard deviations of these quantities due to the scattering of the experimental data. Figure 22 shows the experimental points and analytical curve of one of the radial flux distributions obtained by fuel rod scanning. Figure 23 presents the same information for one of the axial flux distributions also obtained by fuel rod scanning.

By subtracting the actual core radius or height from the corresponding extrapolated quantities, the value of the radial or axial reflector savings was found. A total of 16 radial and 10 axial determinations were made. No significant systematic differences were observed in the radial reflector savings obtained by the different methods. However, for the axial reflector savings, the foil measurements yielded values consistently smaller than those obtained from fuel rod scanning. This difference has not been resolved.

The average values of the reflector savings were obtained by weighting each individual value according to the inverse square of its standard deviation. For the radial reflector savings, the standard deviation for the average was found by the same weighting process. However, the error assigned to the axial reflector savings includes an allowance for the systematic difference just mentioned. The values found were

$$\lambda_r = 7.0 \pm 0.3 \text{ cm} \quad (39)$$

$$\lambda_h = 6 \pm 1 \text{ cm} \quad (40)$$

When these are combined with the values previously given for R and H , one obtains upon substitution in Eq. 37 above:

$$B_r^2 = (50.6 \pm 0.8) \times 10^{-4} \text{ cm}^{-2} \quad (41)$$

$$B_h^2 = (5.5 \pm 0.2) \times 10^{-4} \text{ cm}^{-2} \quad (42)$$

and
$$B^2 = (56.1 \pm 1.0) \times 10^{-4} \text{ cm}^2 \quad (43)$$

Control Rod Worth

The hold-down worth of a centrally located control rod of silver-cadmium (69.83 wt % Ag, 30.15 wt % Cd) was measured by a differential method. The differential worth ($\Delta k/k$ per centimeter) was determined as a function of the length of the control rod inserted into the reactor. Since this process involved the addition of fuel and thus an increase in the core size, an analytical correction had to be applied to normalize each measurement to the just critical core size which was 1874 fuel rods with the central control rod in place and fully withdrawn at a temperature of 14°C. The resulting curve is shown in Fig. 24. This differential curve was then graphically integrated to obtain the integral hold-down worth. This integral curve is also given in Fig. 24. The total hold-down worth was found to be $7.3 \pm 0.3\%$ $\Delta k/k$.

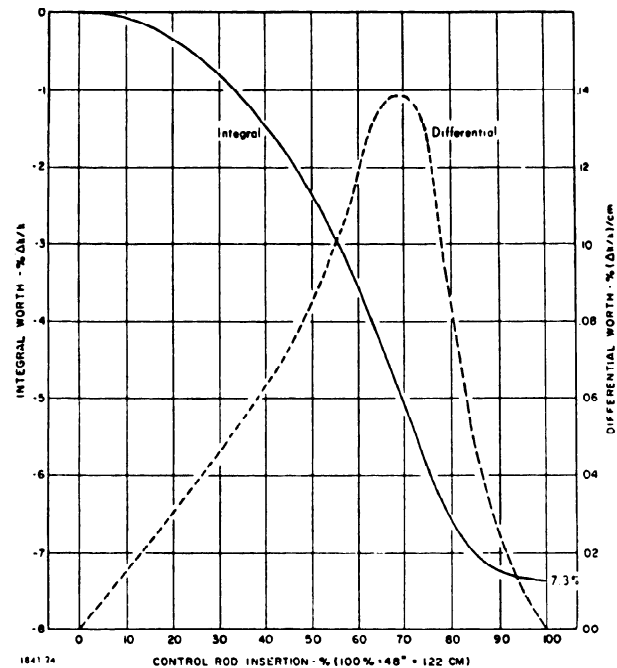


Figure 24. Central control rod—Yankee critical experiments—3 : 1 core (corrected to just critical core of 1874 fuel rods)

ACKNOWLEDGEMENTS

It is only because of the efforts and assistance of many persons in the Westinghouse Atomic Power Department that the results reported here could be obtained. It is not possible to mention the names of all of them. We are especially indebted to W. E.

Abbott, G. M. Inman, H. W. Graves, Jr., W. H. Arnold, Jr., J. Jedruch, R. D. Edsell and G. H. Eng of the Reactor Engineering Department; R. K. McGeary, D. G. Brunstetter and E. S. Foster of the Nuclear Core Engineering Department; M. River, W. J. Miller, Jr., R. B. Shomo, and J. P. Tobin of the Reactor Evaluation Center.

REFERENCES

1. H. Kouts, G. Price, K. Downes, R. Sher and V. Walsh, *Exponential Experiments with Slightly Enriched Uranium Rods in Ordinary Water*, Proceedings of the International Conference on the Peaceful Uses of Atomic Energy, Geneva 1955, P/600, Vol. 5, p. 183, United Nations, New York (1956).
2. H. Kouts and R. Sher, *Experimental Studies of Slightly Enriched Uranium, Water Moderated Lattices*, BNL-486 (1958).
3. M. B. Egiazarov, V. S. Dikarev and V. G. Madeev, *Conference of the Academy of Sciences of the USSR on the Peaceful Uses of Atomic Energy—Session of Physical and Mathematical Sciences* (1955).
4. J. P. Anthony, P. Bacher, Mme. L. Heureau, J. Moreau and A. P. Schmitt, *Measure de l'absorption Resonante*, CEA Report no. 670 "1" (1957).
5. D. Klein et al., *Measurements of Thermal Utilization, Resonance Escape Probability, and Fast Effects in Water Moderated, Slightly Enriched Uranium and Uranium Oxide Lattices*, Nuclear Sci. and Eng. (April 1958).
6. S. Krasik and A. Radkowsky, *Pressurized Water Reactor (PWR) Critical Experiments*, Proceedings of the International Conference on the Peaceful Uses of Atomic Energy, Geneva 1955, P/601, Vol. 5, p. 203, United Nations, New York (1956).
7. A. M. Weinberg and L. C. Noderer, *Theory of Neutron Chain Reactions, Vol. I, Diffusion and Slowing Down of Neutrons*, CF-51-5-98 (May 1951).
8. W. H. Arnold Jr., *Analysis of Experimental Data on Reactivity of Plutonium-Bearing Fuel Rods*, YAEC-57 (1958).
9. Glasstone and Edlund, *Elements of Nuclear Reactor Theory*, p. 194, D. Van Nostrand Co., New York (1955).
10. H. J. Amster, *The Wigner-Wilkins Calculated Thermal Neutron Spectra Compared with Measurements in a Water Moderator*, Nuclear Sci. and Eng., 2, 394 (1957).
11. M. J. Poole, *Measurements of Neutron Spectra in Moderators and Reactor Lattices*, J. Nuclear Energy, 5, 325 (1957).
12. E. D. Clayton, *Epicadmium Fissions in U²³⁵*, HW-35729 (1955).
13. G. R. Keepin, T. F. Wimett and R. K. Zeigler, *Delayed Neutrons from Fissionable Isotopes of Uranium, Plutonium and Thorium*, Phys. Rev. 107, p. 1044 (1957).
14. R. Batchelor and H. R. McK. Hyder, *The Energy of Delayed Neutrons from Fission*, J. Nuclear Energy, 3, 7 (1956).
15. Edlund, Wehmeyer, Secrest and Williams, *Physics of Water Moderated Thorium Reactors*, unpublished manuscript.
16. Dayton and Pettus, *The Effective Resonance Integral of Thorium and Thorium Oxide*, N.S.E., 286 (1958).